Journal of Engineering Mathematics **43:** 281–314, 2002.
© 2002 *Kluwer Academic Publishers. Printed in the Netherlands.*

Models for gravitationally-driven free-film drainage

R. J. BRAUN*, S. A. SNOW[1] and S. NAIRE[2]
[1]*Department of Mathematical Sciences, University of Delaware, Newark, DE 19716, USA; *Author for correspondence (Fax (302)831-4511; Email: braun@math.udel.edu)*
[2]*Interfacial Expertise Center, Dow Corning Corporation, Midland, MI 48686-0994, USA*
‡*University of Delaware; Current address: Division of Theoretical Mechanics, School of Mathematical Sciences, University of Nottingham, University Park, Nottingham NG7 2RD, UK*

Received 4 July 2001; accepted in revised form 3 May 2002

Abstract. The drainage of the thin fluids layers, or lamellae, in a foam may be modeled by a vertical draining thin liquid film. A sequence of mathematical models is described that attempts to explain some aspects of the drainage of the film. Lubrication theory is used to derive the nonlinear partial differential equations (PDE) that describe the film; all models assume an insoluble surfactant in this paper. The models include effects from gravity, viscosity, surface tension and its dependence on surface concentration (the Marangoni effect), and surface viscosity; they may also include nonlinear equations of state. The models are able to predict very well the fast and slow limits of the drainage observed experimentally; a limited range of intermediate drainage rates has been described by these models to date. The limitations of the models and possible extensions will be discussed.

Key words: film drainage, insoluble surfactant, lubrication theory.

1. Introduction

Soap films have fascinated scientists and laymen for hundreds of years; they are important models for a number of scientific and technological phenomena including the stability of foams, emulsions, and other disperse systems, the mathematical construction of geometrical figures with minimal surface area, and the structure and stability of biological membranes (*e.g.*, [1–3]). These films are visually fascinating due to the intense light interference band colors of the film and their rapid and turbulent flow patterns.

The drainage of soap films has been studied by a number of authors (*e.g.*, [1, 4]). A variety of phenomena may be of interest, including details of rupture (for a recent review, see [5], the drainage of films with micelles present (*e.g.*, [6, 7, 8]) or with non-Newtonian surface properties [9, 10]. Drainage of thin films is important in foams, where the properties of foam as a material may be of interest (*e.g.*, [11, 12]), or where understanding of the behavior on a smaller scale may be desired [13].

A number of authors have examined thinning of lamella in foams [6–9]; in these papers the lamella is assumed to be flat and a force balance is used instead of the normal-stress condition. These works have successfully shown the role of a number of physical effects in drainage of lamella. However, in this work we are very interested in the deformation along the film as a part of the solution. Miller and coworkers have studied axisymmetric lamella drainage with a deformable surface, without the influence of gravity [14, 15]. The stability of a vertically-oriented soap film was studied in a similar manner by Bruinsma [16]. The flow of a lamella into a meniscus in a foam was studied using matched asymptotic expansions by Breward [17]. They analysed the drainage with and without surface viscosity in the presence

Table 1. The volumetric rate of polyurethane film drainage as a function of TCP concentration in parts per million (PPM).

[TCP] (ppm)	Film drainage rate ($\times 10^4$) (mm^3/min)
10	695
60	311
120	33
330	7

of the Marangoni effect and surfactant transport, and they were able to compute exponents for power law thinning rates.

Our specific interest was in the use of films to model the stability of foam, in particular, some effects of surfactants on foam stability. The foam system that we concentrated on was polyurethane foam, the surfactants that we studied were silicone based surfactants. Polyurethane foam is a multi-billion-dollar-per-year technological and commercial undertaking. Silicone-based surfactants are necessary for the production of this type of foam. The behavior of these surfactants in polyurethane foams was recently reviewed by one of the authors [18].

The premise of our work was that operational polyurethane foam, a complex physico-chemical system, could be adequately modeled by employing draining, vertical liquid films. This premise had been previously employed by many workers in the area of aqueous-based foam and films. Addition of surfactant is necessary to the polyurethane foam-fabrication process in order to preserve the long thin films which drain into the Plateau borders (*e.g.*, [19, Chapter 7]); achieving an optimal rate of drainage by use of the proper surfactant is necessary for effective and efficient production of foam. Film drainage which is too rapid leaves one with a foam of insufficient volume and excessive porosity.

The behavior of surfactants within a foam of film is complex. A key necessity of the surfactant is to strongly adsorb at the liquid/air interface. In fact, the molecular structure of the surfactant is specified to achieve this goal. Individual surfactant molecules adsorb at the interface and then aggregate together to form a coherent monolayer at that interface. There are a number of mechanical consequences of the monolayer formation. Firstly, the interfacial (surface) tension is systematically lowered as a function of surfactant interfacial concentration, until a saturated condition is achieved. However, within a dynamic system such as a film there is the constant creation of gradients of surface concentration and therefore surface tension. Through bulk and surface transport of surfactants there is a constant effort to relieve these gradients. Secondly, the mechanical coherence of the surface gives rise to shear and dilational surface viscosities.

The interfacial stresses created from interfacial tension gradients and surface viscosity are necessary to control film-drainage rate, and therefore, foam stability. At the high extremes of gradients and viscosity, the surface of the film becomes rigid, or tangentially immobile (*e.g.*, [20]). This behavior results in exceptionally low film-drainage rates and stable (usually overtly-stabilized) foam. In concept, the rate of film drainage, as a function of the surfactant effect on interfacial stresses, can be precisely controlled by specification of the molecular structure and concentation of the surfactant. We have demonstrated this in practice as shown in Table 1 below. The surfactant employed is labelled TCP. The decrease of the film-drainage rate

with increase in TCP concentration is consistent with a widely accepted physical model where the increase in surface concentration translates into the formation of a more mechanically coherent surface monolayer, therefore, a higher surface viscosity and ultimately, a lower film-drainage rate. Furthermore, as the TCP concentration was increased, the (Marangoni) flow patterns on the film surface progressively decreased in both rate and intensity; this is further evidence of the rigidifying of the surface of the film with an increase in TCP concentration. On this basis we chose to include surface viscosity and Marangoni effects in the computational model. Finally, the range of film thicknesses in these experiments spanned the range from 0·2 mm to tenths of microns; intermolecular forces may be expected to be significant for film thickness on the order of a few hundred nanometers. Therefore, intermolecular forces between the film surfaces were not included in the model formulation.

In our experiments, a vertically-oriented rectangular wire frame was dipped into a solution and was then lifted to a fixed height above a cuvette of liquid [21]. Therefore, a thin liquid film was suspended from the wire frame to the 'bath' in the cuvette, and it subsequently drained back into the bath. The bath was designed to model the Plateau border; the top of the film was designed to model the middle of a film in a foam. The model most closely approximated a vertically-oriented lamella with a border at the bottom, but the results were sufficiently applicable that useful conclusions were made about the effectiveness of surfactants in foam fabrication as discussed below. Details of the experiment appear elsewhere [21, 22]; the experiment is very similar in configuration to that of Hudales and Stein [23, 24].

In a pioneering study, Mysels *et al*. [1] gave a description of the draining and thinning of vertical aqueous soap films. They found that film surfaces could become immobile and take the shape of downward opening parabolas (concave inward toward the midplane of the film). These films tended to be several microns thick and drain relatively slowly. For relatively small surfactant concentration the film boundaries were 'mobile'; these films drained quickly and were concave outward (from the midplane of the film). Mysels *et al*. called these shapes 'hollow ground.' When the wire frames had vertical sides, sideways flow into the Plateau borders at the edges of the film was observed. The flow in the border regions, where thin spots of film are generated and thicker spots disappear, was termed 'marginal regeneration'.

In Hudales and Stein's work [23−25], both two- and three-dimensional features of aqueous films were measured, and the results were compared with theory that they developed in a manner similar to Mysels *et al.* [1, Chapter 5]. They were interested in two-dimensional film profiles, the three-dimensional shapes of the films, and marginal regeneration at their edges. In [24, 25], time-independent lubrication-like approximations for the flow in a two-dimensional horizontal slice of the film were developed. Assumed surface velocity and flow-rate data were input into this model; film profiles for the transition zone from the film into a vertical Plateau border were given in [25]. They concluded that their model equations gave good approximations but were not exact; the approximations did not treat the time evolution of the films.

Nierstrasz and Frens [26, 27] proposed Marangoni effects as a cause for structures observed at the edges of vertical films, and they developed a computational model of the draining film. Their model is two dimensional, includes a soluble surfactant and seems to be focussed on the region where the film meets the surface of the bath; the film part of the model takes up about a quarter of the computational domain, with the Plateau border region taking up the remainder. This is in contrast to our work [28−31] where the entire film above the transition zone and transition zone are combined into a single model with the film forming the vast majority of the computational domain. Their computations [27] apparently exhibit jumps of the slope in the

surface velocity, and localized spikes in the surface concentration, at a point in the transition area (inside the computational domain). They also speculate that the Marangoni effect may cause instability of the film near the bath leading to what they call ‘peacock feather’ structures [1, p. 12] at the bottom of a vertical draining film. These finger-like structures climb up the film and tend to slow down and widen away from the bath in aqueous solutions; the corresponding structures in polyurethane films is much wider and slower than in aqueous films. We concur with their idea that these structures are due to the competition between Marangoni and gravity effects, but we differ in the mathematical approach to the problem.

The evolution of a vertically-oriented soap film entirely enclosed in a frame was studied by Schwartz and Roy [32]. They observed that different regions develop similar to those suggested in [28]. They also included van der Waals forces and found the formation of thin regions that were interpreted to be black film.

We develop lubrication theory that describes several aspects of this experiment and predicts film shapes during drainage in detail. A set of nonlinear PDEs describing the time-evolution of the fluid interface, tangential component of the surface velocity and the transport of surfactant along the free surface are derived. A systematic study of the relevant parameters is conducted so as to recover a range of experimental observations of Mysels *et al*. [1], as well as those observed by Snow *et al*. [21]. We recover, in the limit of large surface viscosity, the tangentially-immobile case studied previously [28, 33]. For mobile films without large surface viscosity, transition from a mobile to an essentially immobile film is observed for increasing surface-tension gradients. This behavior has been observed in several different physical situations: levelling of a thin liquid-coating layer [34, 35], the dip-coating problem in the presence of an insoluble surfactant [36] and a tangentially-immobile region of a drop with a monolayer of insoluble surfactant deforming in an axisymmetric extensional flow [37, 38]. The models discussed in this paper will show how both rigid and mobile behavior can be obtained in the vertical film context with either significant surface viscous or Marangoni effects.

In Section 2.1, we give a general two-dimensional formulation of the model we use for the drainage of the vertical free film [30]. This formulation includes both the lubrication theory for the thin film and a connection to the bath below the film. We give results from several cases in succeeding sections that illuminate the results in several limits. In Section 3.1, we give a drastically simplified model (the tangentially-immobile model [28]) and show how it can recover the observations of the slowest draining films [1, 21]. The structures observed there readily serve as a map for interpreting the results that follow. In Section 3.2, we give extended results that show mobile and rigid results which may be obtained by limiting cases of surface tension or Marangoni effects. In Section 3.3, we give results for the case with nonlinear surface properties that are realistic for some aqueous films. In Section 4, we give results [39] that show both analytically and computationally that large surface viscosity recovers the rigid-film limit, while small surface viscosity recovers the mobile, fast-draining limit of the experiments by Snow *et al*. [21]. This last analysis was performed only on the flat middle section of the film where mean surface tension could be neglected and Marangoni effects must be assumed to be weak; this simplification is the only one that requires these assumptions. In Section 5, we discuss the models and outline areas for improvement.

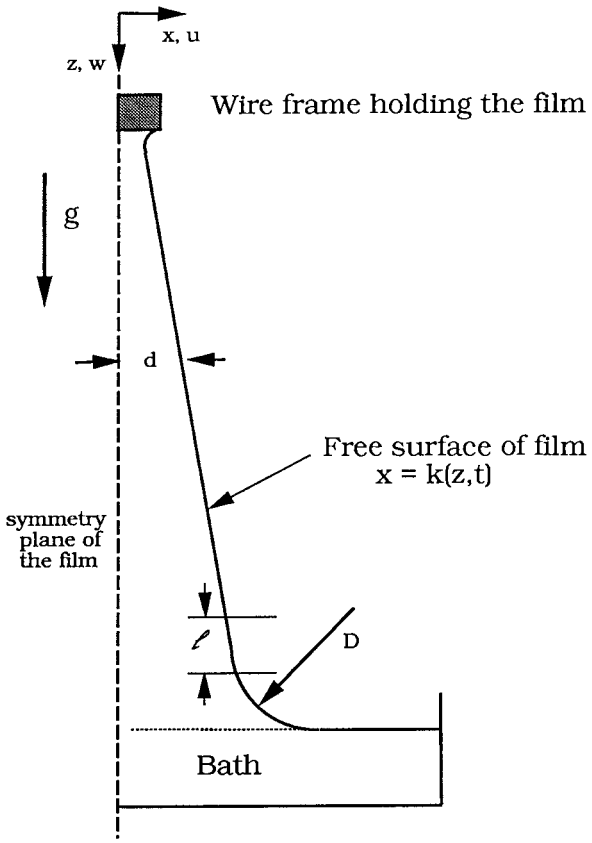

Figure 1. Schematic representation of the problem studied. Here d is a characteristic film thickness where gravitational and viscous forces balance; D is the static meniscus radius where gravitational and surface-tension forces balance; $\ell = d^{1/3}D^{2/3}$ is a length scale where all three forces balance.

2. Two-dimensional models

We begin with a derivation for the two-dimensional geometry with nonlinear surface properties. The model will be reduced to various special cases in order to illuminate the roles played by various effects in succeeding sections as needed.

2.1. General formulation

2.1.1. *Dimensional problem*

Consider a two-dimensional draining film in a Cartesian coordinate system $(\bar{x}, \bar{z})$ (see Figure 1); it is hanging from a thin plate at $\bar{z} = 0$. Gravity acts in the downward direction so $\mathbf{g} = g\mathbf{k}$, where $\mathbf{k}$ is the unit vector pointing in the positive $\bar{z}$ direction. The free surface of the thin film is given by $\bar{x} = \bar{k}(\bar{z}, \bar{t})$ and the top end of the film is assumed to be fixed at $\bar{k} = k_0$. The film is assumed to be symmetric about the line $\bar{x} = 0$ (the $\bar{z}$ axis). The equations of motion and boundary conditions are

$$\bar{\nabla} \cdot \bar{\mathbf{v}} = 0, \tag{1}$$

$$\rho\left(\frac{\partial \bar{\mathbf{v}}}{\partial \bar{t}} + \bar{\mathbf{v}} \cdot \bar{\nabla}\bar{\mathbf{v}}\right) = \mu\bar{\nabla}^2\bar{\mathbf{v}} - \bar{\nabla}\bar{p} + \rho g\mathbf{k}; \tag{2}$$

where $\mathbf{k} = (0, 1)$, $\bar{\mathbf{v}} = (\bar{u}, \bar{w})$ is the velocity vector and $\bar{p}$ is the pressure. Here g is the magnitude of gravitational acceleration, ρ is the density and μ is the dynamic shear viscosity of the fluid. We assume that ρ and μ are constant.

Boundary conditions for (1) and (2) include the (assumed) symmetry condition at $\bar{x} = 0$ given by

$$\bar{u} = \bar{w}_{\bar{x}} = 0. \tag{3}$$

The instantaneous location of the free surface $\bar{x} = \bar{k}(\bar{z}, \bar{t})$ is described by the kinematic boundary condition

$$\bar{u} = \bar{k}_{\bar{t}} + \bar{k}_{\bar{z}}\bar{w}. \tag{4}$$

The normal and the tangential component of the interfacial stress is derived from the Boussinesq-Scriven surface-stress model [40] and is given by [41, Section 4.2], [42]

$$-\bar{\mathbf{n}}\cdot \parallel \bar{\mathcal{T}} \parallel \cdot\bar{\mathbf{n}} = 2\bar{\mathcal{H}}\bar{\sigma} + 2\bar{\mathcal{H}}(\kappa^{\mathbf{s}} + \mu^{\mathbf{s}})\bar{\nabla}_{\mathbf{s}}\cdot\bar{\mathbf{v}}, \tag{5}$$

$$-\bar{\mathbf{t}}\cdot \parallel \bar{\mathcal{T}} \parallel \cdot\bar{\mathbf{n}} = \bar{\mathbf{t}}\cdot\bar{\nabla}_{\mathbf{s}}\bar{\sigma} + (\kappa^{\mathbf{s}} + \mu^{\mathbf{s}})\bar{\mathbf{t}}\cdot\bar{\nabla}_{\mathbf{s}}\bar{\nabla}_{\mathbf{s}}\cdot\bar{\mathbf{v}} + \bar{\bar{t}}\cdot\boldsymbol{\nabla}_{\mathbf{s}}\left(\kappa^{\mathbf{s}} + \mu^{\mathbf{s}}\right)\boldsymbol{\nabla}_{\mathbf{s}}\cdot\bar{\mathbf{v}}, \tag{6}$$

respectively, for variable surface viscosities. Here, $\bar{\mathbf{n}}$ is the unit outward surface normal and $\bar{\mathbf{t}}$ is the unit tangent vector along the free surface. $\parallel \bar{\mathcal{T}} \parallel = \bar{\mathcal{T}}_{\mathbf{a}} - \bar{\mathcal{T}}$ denotes the jump in the stress tensor across the free surface where $\bar{\mathcal{T}} = -\mathbf{I}\bar{p} + \mu(\bar{\nabla}\bar{v} + \bar{\nabla}\bar{v}^{t})$ is the stress tensor and $\bar{\mathcal{T}}_{\mathbf{a}}$ is the stress tensor in the outside air phase (assumed to be zero). $\bar{\mathcal{H}}$ is the mean curvature of the free surface, $\bar{\sigma}$ is the surface tension, $\kappa^{\mathbf{s}}$ and $\mu^{\mathbf{s}}$ are the surface dilatational and shear-viscosity coefficients, respectively, and $\bar{\nabla}_{\mathbf{s}}$ denotes the surface-gradient operator. Surface-differentiation operators are based on [40, 43, 44].

Accurate surface viscosity measurements for silicone surfactants in polyurethane are difficult to find at best. These properties may be profitably investigated by the methods of Hirsa and Lopez [45, 46] using a deep-channel viscometer and by Fuller and co-workers [47, 48] using a needle viscometer. These methods can reliably determine the surface shear viscosity $\mu^{\mathbf{s}}$; the surface dilatational viscosity $\kappa^{\mathbf{s}}$ remains difficult to measure as, for instance, discussed in [41, Chapter 8]. The only description we have of them at this time is that their surface viscosity can be very high for some surfactants. We choose a form similar to that measured by Hirsa and Lopez [45, 46]. The functional form used is

$$\kappa^{\mathbf{s}} + \mu^{\mathbf{s}} = (\kappa^{\mathbf{s}} + \mu^{\mathbf{s}})_m G(\alpha_1\Gamma), \tag{7}$$

where $(\kappa^{\mathbf{s}} + \mu^{\mathbf{s}})_m$ is a the surface viscosity evaluated at the reference concentration $\bar{\Gamma}_m$ and Γ is the surfactant concentration. (For hemicyanine on water, the reference value would be $\Gamma_m = 0{\cdot}856$ mg/m^2 [46].) $G(\alpha_1\Gamma)$ is a dimensionless nonlinear function of Γ such that $G(0) = 0$. For our numerical calculations, we use

$$G = -1 + \exp(\alpha_1\Gamma). \tag{8}$$

For Γ close to zero, G is small and increases with Γ.

For the case when the fluid surface contains a dilute insoluble surfactant, surface tension is no longer a constant and is assumed to behave according to

$$\bar{\sigma} = \bar{\sigma}_m + \beta F(\alpha\Gamma), \tag{9}$$

where $\bar{\sigma}_m$ is the surface tension evaluated at the reference concentration $\bar{\Gamma}_m$. β and α (typically $\alpha < 0$) are constant material parameters which are related to the range in $\bar{\sigma}$ and to the slope of the equation of state at the inflection point, respectively. The range of concentration allowed is from that of a clean surface to that of some other state. The other state could be a saturated surface, or is more likely a phase change as in [45, 46]. $F(\alpha\Gamma)$ is a dimensionless function which represents a nonlinear deviation of $\bar{\sigma}$ from $\bar{\sigma}_m$. For our numerical calculations, we use an equation of state for surface tension similar to the one used by Hirsa and Lopez [45, 46], *i.e.*,

$$\begin{aligned} \bar{\sigma} &= \bar{\sigma}_m + \beta \tanh\left[\alpha(\Gamma - 1)\right], \\ F &= \tanh\left[\alpha(\Gamma - 1)\right], \quad (\alpha < 0). \end{aligned} \tag{10}$$

The nearly flat behavior for small Γ that is implied by this formula is typical of insoluble surfactants [49]. The inflection point is at $\Gamma = 1$; this is the region where the surface-tension gradients are maximum. Hirsa and Lopez [45, 46] have measured surface tension up to $\Gamma = 1$, beyond which their water/hemicyanine system appears to undergo a phase transistion; we similarly consider $\Gamma \leq 1$. Generally, such detailed measurements are not available for polyurethane with silicone surfactant; for a recent review see Snow *et al*. [18].

The transport equation for the surfactant on the free surface is [40, 43, 44]

$$\frac{\partial \bar{\Gamma}}{\partial \bar{t}} + \bar{\nabla}_s \cdot \left(\bar{\Gamma}\bar{\mathbf{v}}\right) = \mathcal{D}_s \bar{\nabla}_s^2 \bar{\Gamma} - \mathbf{n} \cdot \mathbf{j}, \tag{11}$$

where the surface concentration of surfactant is $\bar{\Gamma} = \bar{\Gamma}\left(\bar{k}(\bar{z}, \bar{t}), \bar{z}, \bar{t}\right)$ and $\mathcal{D}_s$ is the surface diffusivity. Here, $-\bar{\mathbf{n}} \cdot \mathbf{j}$ is the flux of the surfactant between the bulk and the free surface, for the insoluble case, $\mathbf{j} = \mathbf{0}$.

2.1.2. *Nondimensionalization*

We will use length scales based on the tangentially-immobile case [28, 50]. The three length scales are

$$d = \sqrt{\frac{\mu W}{\rho g}}, \qquad D = \sqrt{\frac{\bar{\sigma}_m}{\rho g}} \qquad \text{and} \qquad \ell = d^{1/3} D^{2/3}; \tag{12}$$

they are the film thickness d, equilibrium meniscus radius D, and the intermediate scale ℓ, respectively. The velocity scale

$$W = \rho g d^2 / \mu \tag{13}$$

balances the shear across the film with the gravitational term in the vertical momentum equation to appear below when the surface is immobile. The equilibrium mensicus radius balances gravity and surface tension. ℓ is a length scale which balances viscous, gravitatonal and surface tension forces, and has appeared in the context of the dragout problem [50]. Using an experimentally determined value for d, the corresponding vertical velocity scale is given by solving for W. Separation of scales occurs with

$$\delta^2 = \frac{d}{\ell} \ll 1. \tag{14}$$

We then introduce the following nondimensionalizations

$$x = \frac{\bar{x}}{d}, \quad z = \frac{\bar{z}}{\ell}, \quad t = \frac{W}{\ell}\bar{t}, \quad u = \frac{\bar{u}}{\delta^2 W}, \quad w = \frac{\bar{w}}{W}, \quad k = \frac{\bar{k}}{d},$$
$$p = \frac{\delta^4 \ell}{\mu W}\bar{p}, \quad \Gamma = \frac{\bar{\Gamma}}{\bar{\Gamma}_m}, \quad \sigma = \frac{\bar{\sigma}}{\bar{\sigma}_m}. \tag{15}$$

Substitution of the above dimensionless variables in the equations governing the flow inside the film (Equations (1) and (2)) furnishes the following dimensionless problem. Inside the film, we have

$$u_x + w_z = 0, \tag{16}$$

$$\delta^8 \mathcal{R}(u_t + uu_x + wu_z) = \delta^4(u_{xx} + \delta^4 u_{zz}) - p_x, \tag{17}$$

$$\delta^4 \mathcal{R}(w_t + uw_x + ww_z) = w_{xx} + \delta^4 w_{zz} - p_z + 1. \tag{18}$$

On the plane $x = 0$, symmetry requires $u = w_x = 0$; on the free surface of the film, we have a nondimensional surfactant transport equation given by

$$\Gamma_t + N^2\left[\delta^4 k_z \mathcal{A}(\Gamma u) + \mathcal{A}(\Gamma w)\right] = \frac{1}{\mathcal{P}}\left[(\delta^2 N^2 k_z \mathcal{A})^2 + (N^2 \mathcal{A})^2\right]\Gamma, \tag{19}$$

where

$$N := \frac{1}{\sqrt{1 + \delta^4 k_z^2}} \quad \text{and} \quad \mathcal{A} := k_z \frac{\partial}{\partial x} + \frac{\partial}{\partial z}. \tag{20}$$

The kinematic condition becomes

$$k_t - u + k_z w = 0; \tag{21}$$

the tangential and normal components of the interfacial stress condition can be written as

$$\begin{aligned} N^2\left[2\delta^4 k_z(u_x - w_z) + (\delta^4 u_z + w_x)(1 - \delta^4 k_z^2)\right] &= -N\frac{\mathcal{M}}{\alpha}\mathcal{A}F \\ &\quad + \mathcal{S}G\left[N\mathcal{A}(N^2\delta^4 k_z \mathcal{A}u + N^2 \mathcal{A}w)\right] \\ &\quad + N^3 \mathcal{S}\mathcal{A}G(\delta^4 k_z \mathcal{A}u + \mathcal{A}w) \end{aligned} \tag{22}$$

and

$$\begin{aligned} &\frac{\delta^6}{\mathcal{C}} k_{zz} N^3\left[1 + \delta^4 \frac{\mathcal{M}}{\alpha}F + \delta^4 N^2 \mathcal{S}G(\delta^4 k_z \mathcal{A}u + \mathcal{A}w)\right] = \\ &\qquad 2\delta^4 N^2\left[u_x + \delta^4 k_z^2 w_z - k_z(\delta^4 u_z + w_x)\right] - p, \end{aligned} \tag{23}$$

respectively. In our scalings, $\mathcal{C} = \delta^6$ and so the leftmost term in (23) is of unit order. Several dimensionless groups have appeared and they are listed in Table 2. For the choice of $\bar{\sigma}$ given in (10), we have $\mathcal{M} = -\beta\alpha\delta^2/(\mu W)$.

In this work, we wish to study a range of parameter values, in particular for varying $\mathcal{M}$ and $\mathcal{S}$. We are interested primarily in a viscous fluid that is about 80 times as viscous as water, but it is relatively easy to find parameters for aqueous systems. We shall find that the values of $\mathcal{M}$ may be considered small for values less than about 30, and that $\mathcal{S}$ may be considered small

Table 2. Table of nondimensional parameters and their interpretations. Note that in our scalings $\mathcal{C} = \delta^6$ (see 29, 39]).

Number	Definition	Comparison of forces
Reynolds	$\mathcal{R} = \frac{\rho W \ell}{\mu}$	$\frac{\text{inertial}}{\text{viscous shear}}$
Modified Boussinesq	$\mathcal{S} = \frac{(\kappa^s + \mu^s)_m W/\ell^2}{\mu W/d}$	$\frac{\text{surface viscous shear}}{\text{viscous shear}}$
Capillary	$\mathcal{C} = \frac{\mu W}{\bar{\sigma}_m}$	$\frac{\text{viscous shear}}{\text{surface tension}}$
Marangoni	$\mathcal{M} = \frac{-\left(\frac{\partial \sigma}{\partial \Gamma}\right)_m \Gamma_m}{\mu W} \delta^2$	$\frac{\text{concentration gradient shear}}{\text{viscous shear}}$
Péclet	$\mathcal{P} = \frac{W \ell}{\mathcal{D}_s}$	$\frac{\text{advective transport}}{\text{diffusive transport}}$

for values of 100 or less. For the parameters given in [39], $\mathcal{M}$ could be as large as 700 and $\mathcal{S}$ ranged from about 50 to more than 10^4. The Reynolds number is on the order of 10^{-7}, while for thicker films it could be as much as 10^{-5}; it may thus be considered small. The Péclet number is on the order of 10^4; surface diffusion will be neglected in a number of cases that follow. For the films of interest to us, the value of δ is typically around 10^{-1}.

2.2. Lubrication theory

We look for solutions in the form of a regular perturbation expansion in powers of δ^4:

$$(u, w, k, p, \Gamma) = (u, w, k, p, \Gamma)^{(0)} + \delta^4 (u, w, k, p, \Gamma)^{(1)} + \ldots \tag{24}$$

Substituting the series expansions in the non-dimensional equations gives to leading order in the bulk (inside the film)

$$u_x^{(0)} + w_z^{(0)} = 0, \tag{25}$$

$$0 = -p_x^{(0)}, \tag{26}$$

$$0 = w_{xx}^{(0)} - p_z^{(0)} + 1. \tag{27}$$

These are subject to the symmetry condition at $x = 0$,

$$u^{(0)} = w_x^{(0)} = 0. \tag{28}$$

At $x = k^{(0)}(z, t)$ we have

$$k_t^{(0)} - u^{(0)} + k_z^{(0)} w^{(0)} = 0, \tag{29}$$

$$-\frac{\mathcal{M}}{\alpha} \mathcal{A} F + \mathcal{S} G \left[\mathcal{A} (N^2 \delta^4 k_z^{(0)} \mathcal{A} u^{(0)} + N^2 \mathcal{A} w^{(0)}) \right] + N^2 \mathcal{S} \mathcal{A} G \left(\delta^4 k_z^{(0)} \mathcal{A} u^{(0)} + \mathcal{A} w^{(0)} \right) = N w_x^{(0)}, \tag{30}$$

$$\kappa^{(0)} = -p^{(0)}, \tag{31}$$

where

$$\kappa^{(0)} = k_{zz}^{(0)} N^3 = \frac{k_{zz}^{(0)}}{\left(1 + \delta^4 {k_z^{(0)}}^2\right)^{3/2}} \tag{32}$$

is the curvature of the film. Previous work [51, 52] has shown that it is possible to keep the full curvature in the normal-stress condition and integrate through the matching region onto the static meniscus; our model relies on those results. In a strict asymptotic sense, this is not valid; on the other hand, the stress conditions contain all the terms necessary to match the film onto the meniscus.

Using Equations (27), (31) and symmetry at $x = 0$, we obtain

$$w^{(0)} = -(1 + \kappa_z^{(0)})\frac{x^2}{2} + B(z, t). \tag{33}$$

We define

$$w^{(S)}(z, t) := \left[-(1 + \kappa_z^{(0)})\frac{{k^{(0)}}^2}{2} + B \right], \tag{34}$$

where $w^{(S)}$ is the velocity along the free surface. Equation (30), after dropping the superscript $^{(0)}$, becomes

$$\mathcal{S}\left(G w_z^{(S)}\right)_z + \frac{1}{N} k(1 + \kappa_z) - \frac{1}{N^2}\mathcal{M} F_\Gamma \Gamma_z = 0. \tag{35}$$

From the kinematic condition we obtain

$$k_t + \left[k w^{(S)} + \frac{k^3}{3}(1 + \kappa_z) \right]_z = 0. \tag{36}$$

This evolution equation is coupled with the equation for surface velocity, Equation (35) and the surfactant transport equation given by

$$\Gamma_t + N^2 \left[\Gamma w^{(S)} - \frac{1}{\mathcal{P}} N^2 \Gamma_z \right]_z = 0. \tag{37}$$

We have retained some normalization factors, *i.e.*, powers of N, in both the surface velocity and the surface transport equation for Γ, because we kept the full curvature term, κ. These factors would normally be unity from standard lubrication theory. *Post facto* justification for retaining the normalization terms has been given in [29]. Thus the leading-order problem is governed by Equations (35)–(37).

By incorporating surface viscous effects into our model, we have a set of nonlinear PDEs at leading order that fully describe the evolution of the free surface. While retaining inertial terms near rupture is desirable [53–57], we do not believe these terms are important in our situation because we are not near rupture. By the definition of surface velocity, $w^{(S)}(z, t)$, we have introduced a natural variable; retaining the unknown $B(z, t)$ causes fifth-order derivatives of k to appear. Such higher-order derivatives would make our computations to follow much more difficult. This type of formulation has been used in [58], for example.

2.2.1. *Boundary conditions*

Boundary conditions for the film thickness, $k(z, t)$, surface velocity, $w^{(S)}(z, t)$, and the surfactant concentration, $\Gamma(z, t)$, are specified as follows.

At the upper end of the film, *i.e.* $z = 0$, we specify $k(0, t) = 1$ because the film is assumed to be fixed to the wire frame. We also require that there be no flux through the top of the film, which gives us

$$\kappa_z(0, t) = -1, \tag{38}$$

$$w^{(S)}(0, t) = 0. \tag{39}$$

Assuming no surfactant flux at $z = 0$, we have

$$\Gamma_z(0, t) = 0. \tag{40}$$

At the bottom we now must match onto the static meniscus. The virtually static meniscus below is governed by the Young-Laplace equation, *i.e.*,

$$\kappa_z = -1. \tag{41}$$

Solutions of the Young Laplace equation for two-dimensional menisci are parametrized by γ,

$$\frac{\gamma}{\delta^2} = \kappa^2 + \frac{2k_z}{\sqrt{1 + \delta^4 k_z^2}}, \tag{42}$$

a constant in the first integral of Equation (41): for an infinite bath at the bottom of the film, we have $\gamma = 2$. If we think of specifying an initial condition where we fix k_z, we may then use Equation (42) to specify k_{zz} for an infinite bath via

$$k_{zz} = \sqrt{\left(\frac{\gamma}{\delta^2} - 2\frac{k_z}{\sqrt{1 + \delta^4 k_z^2}}\right)(1 + \delta^4 k_z^2)^3}. \tag{43}$$

We specify α and k_z at the bottom of the film, and k_{zz} is then known [42, 52]; these values of k_z and k_{zz} are the boundary conditions for k at the bottom of the film. A typical choice for results given below is the specific choice

$$k_z(L, t) = 10. \tag{44}$$

Imposing k_z and k_{zz} at the end of the domain is an asymptotic 'patch' because the solutions only agree at a single point. In standard matched asymptotics, there is a finite region of overlap between the two solutions. The patching will conserve the amount of surfactant over the film region and it conserves surfactant over the entire fluid surface (union of film and bath surfaces) as may be verified by a simple integration along the fluid surface. However, the surfactant concentration may jump across the patch point from the film side to the meniscus side. We choose to use this approach anyway because this choice will accentuate any effect of surfactant build-up at the bottom of the film as it is washed down during drainage, and we believe this effect may contribute to patterns observed in experiment.

Since the meniscus at the bottom is static, we also have $w^{(S)} = 0$ and no surfactant flux, *i.e.*,

$$\Gamma_z = 0. \tag{45}$$

This furnishes the necessary boundary conditions at the two ends of the film for the model equations.

2.2.2. *Initial conditions*

For all results to follow, we consider the initial shape

$$k(z,0) = 1 + s_0 z, \quad 0 \le z \le L, \tag{46}$$

where $L = 37{\cdot}5$ is the length of the computational domain and $s_0 = 0{\cdot}23$. The initial surfactant concentration is chosen to be either a linear or a hyperbolic tangent function of z; it will be specified in the appropriate section. The variation in the slopes of Γ contributes to the Marangoni effect.

An independent initial condition cannot be specified for the surface velocity; however, for numerical solution we use later, we must find an initial condition that is consistent with those for $k(z,0)$ and $\Gamma(z,0)$.

3. Results for the whole film

3.1. Tangentially immobile film surface

In the limit of large $\mathcal{S}$ or $\mathcal{M}$, the surface tends to become immobile tangentially; details of taking the limit may be found in [28–30, 39]. Briefly, we can consider the tangential-stress boundary condition to be replaced with the kinematic requirement that $\mathbf{t} \cdot \mathbf{v}^{(s)} = 0$; here $\mathbf{t}$ is the unit tangent vector and $\mathbf{v}^{(s)}$ is the velocity of a point in the surface of the film. This forces the surface velocity to be zero; transport of surfactant thus becomes irrelevant. In this limit, we are left with a single nonlinear PDE for the surface of the film. The problem considered and the results given are reported from [28].

3.1.1. *A model for the whole film*

When the average surface tension is significant in the model, a fourth-order nonlinear PDE must be solved, namely,

$$k_t + \left\{ \frac{k^3}{3} \left[\left(\frac{k_{zz}}{\left(1 + \delta^4 k_z^2\right)^{3/2}} \right)_z + 1 \right] \right\}_z = 0. \tag{47}$$

At the upper end of the film we still have $k(0,t) = 1$. We also require that there be no flux through the top of the film, so that

$$\left[\frac{k_{zz}}{(1 + \delta^4 k_z^2)^{3/2}} \right]_z = -1 \tag{48}$$

there for all times.

At the bottom, we must match onto the static meniscus; for this purpose, we use Equation (43) and a specified value of the slope at $z = L$.

In order to solve the problem, we discretize the domain with a uniform grid. Inside the domain, centered finite-difference approximations are used to approximate the spatial derivatives. At the ends, appropriate second-order-accurate finite-difference formulae are used that are not centered. Some details of the boundary treatment are below; full details can be found in [28]. The resulting system of differential equations is then solved using DASSL [59]; this public-domain code provides efficient and robust solution to this stiff problem using adaptive BDF time stepping.

In the numerics to follow we will use the specified slope and the resulting second derivative to determine two fictitious points outside the computational domain, which ends at $z_n = L$. The centered-difference approximation to the second derivative will determine k_{n+1}; a one-sided difference for k_z will determine k_{n+2}. For the numerical approximation at the top of

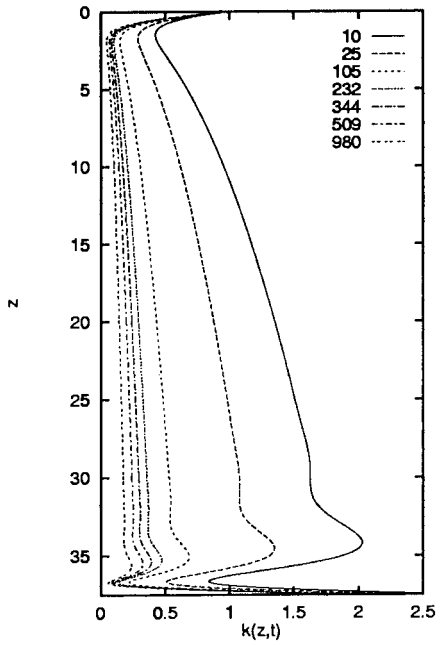

Figure 2. Film shapes $k(z, t)$ *vs.* z with $L = 37{\cdot}5$, $h = 0{\cdot}05$, $k_z(L) = 5$ and $\delta = 0{\cdot}2$. The initial slope of the film was 0·23.

the film, we have two options to solve for the fictitious point k_{-1} at $z = -h$ after using finite-difference formulas of the right form; here h is the mesh spacing. We could (a) solve a nonlinear equation given by the discrete form of the boundary condition or (b) use a perturbation expansion of the boundary condition for $\delta^4 \ll 1$. We used the latter for this work because of its simplicity, and because it was sufficiently accurate for the task at hand. The explicit formula for the ficitious point is then

$$k_{-1} = k_{-1}^{(0)} + \delta^4 k_{-1}^{(4)} + O(\delta^8). \tag{49}$$

The $O(\delta^8)$ terms are neglected; we find

$$k_{-1}^{(0)} = \frac{1}{3}\left(2h^3 + 10k_0 - 12k_1 + 6k_2 - k_3\right) \tag{50}$$

and

$$k_{-1}^{(4)} = \frac{h}{4}\left(k_1 - k_{-1}^{(0)}\right)^2 - \frac{1}{h^2}\left(k_1 - k_{-1}^{(0)}\right)\left(k_1 + k_{-1}^{(0)} - 2k_0\right)^2. \tag{51}$$

The term $k_{-1}^{(0)}$ is identical to that found when one must satisfy the condition $k_{zzz} = -1$ at the top of the film.

The following figures give results for the case of matching past the minimum value of the film thickness. Figure 2 gives the evolution of a film with $k_z(L, t) = 5$ and $\delta = 0{\cdot}2$. There are four distinct regions that may be seen in this time sequence. At the top, there is a meniscus of size ℓ where surface tension, gravity and viscous effects all balance. Below that, there is a region where there is very little curvature; in that region, we shall see that surface tension plays a negligible role. The length of this region is on the order of the static meniscus radius D. Below that, there is a capillary wave which appears to be a sequence of bumps and dips;

we shall discuss that below. Finally, at the bottom there is a static meniscus that is the top of the bath. The length scale of that region is given by D. The formation of these four regions occurs again and again in the sequence of models that we develop here.

The capillary wave above the static meniscus is not an artefact of the numerical solution, but is a solution to the continuous PDE problem. This capillary wave was analyzed in [28], following the analysis of Jensen [60]. The analysis predicts different power laws for the thinning of the relatively flat interior of the film, and for each bump or dip. The exponents for the decay of the thickness of the middle of the film, the highest bump and the deepest dip, were $-0{\cdot}5$, $-0{\cdot}45$ and $-0{\cdot}6$, respectively. The evolution of the bumps and dips is essentially the same as the result from the analysis; the values obtained in the computation were $-0{\cdot}49$, $-0{\cdot}47$ and $-0{\cdot}59$, respectively.

3.1.2. *Further results for the immobile film*

This is just one example of the profitability of viewing the film as composed of separate regions. Section 4 will explore an approximation to the large middle region of the film, where mean surface tension does not contribute to the evolution. Perhaps the most basic fact that one could take away from this view is the following. In order to draw a film, one could estimate the height to raise the frame for the film by computing the static mensicus radius; the height necessary to create a film should be at least a few times larger than this length scale. Further results are given in [28].

3.2. The whole film with constant surface viscosity

We now wish to consider models to where the surface may be mobile or approximately rigid. It is instructive to consider the case where there is a constant surface viscosity and a linearized surface-tension dependence on surface concentration. Following this case, we will consider nonlinear dependence on the surfactant concentration.

For constant surface viscosity we have $G = 1$ and for a linear surface tension we have $F_\Gamma = 1$. We can thus simplify Equations (35)–(37) to obtain

$$\mathcal{S} w^{(S)}_{zz} + \frac{(1+\kappa_z)k}{N} - \frac{\mathcal{M}}{N^2}\Gamma_z = 0, \tag{52}$$

$$k_t + \left[k w^{(S)} + \frac{k^3}{3}(1+\kappa_z) \right]_z = 0, \tag{53}$$

and

$$\Gamma_t + N^2 \left[\Gamma w^{(S)} - \frac{1}{\mathcal{P}} N^2 \Gamma_z \right]_z = 0. \tag{54}$$

Only the equation for the surface viscosity (Equation (35), the tangential-stress condition) has been modified.

The boundary conditions for the film thickness, $k(z,t)$, surface velocity, $w^{(S)}(z,t)$, and the surfactant concentration, $\Gamma(z,t)$, and the film thickness k are the same as those discussed in Section 2.2.1.

In order to solve these nonlinear coupled PDEs we have used a second-order accurate finite-differencing scheme to discretize the spatial derivatives leaving the time derivative continuous. The resulting equations are in the form of a differential-algebraic system; to solve

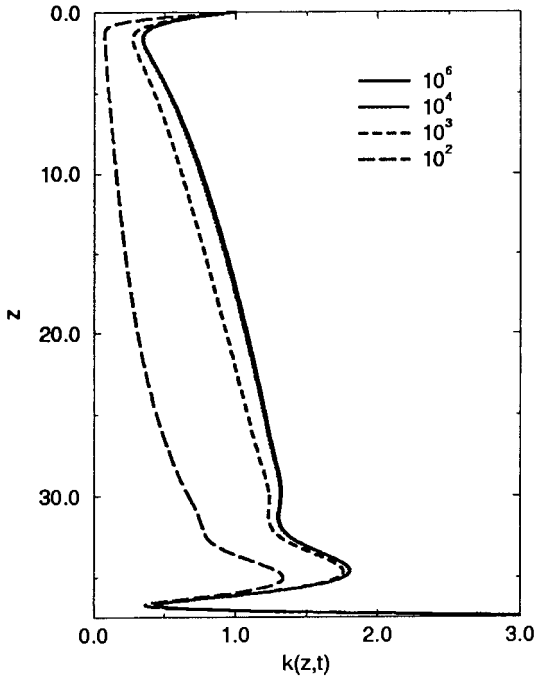

Figure 3. Film shape at $t = 16$ for several $\mathcal{S}$ (upper right). The film is much thinner for small values of $\mathcal{S}$ because the free surface is mobile. For large values of $\mathcal{S}$, the free surface becomes practically immobile.

them we have used the package DASSL [59]. This method will be used to obtain all of the remaining results. For all results to follow, we consider the initial shape $k(z, 0) = 1 + s_0 z$, $0 \leq z \leq L$, where $L = 37{\cdot}5$ is the length of the computational domain and $s_0 = 0{\cdot}23$. A linear free-surface shape is a convenient choice and the choice of initial conditions does not affect the long-time behavior of the film. The initial condition for the surface concentration is

$$\Gamma(z, 0) \equiv \Gamma_0(z) = g_0 + (g_1 - g_0)\frac{z}{L}; \tag{55}$$

here g_0 and g_1, is the surfactant concentration at $z = 0$ and $z = L$, respectively. A consistent initial condition for $w^{(S)}$ must be computed for the code DASSL; solving the discretized equation for $w^{(S)}$, using the initial free-surface shape supplies consistent initial values.

3.2.1. *Constant surface viscosity only*

If we redefine the Marangoni number by $\delta^2\mathcal{M}$ or if $\Gamma = $ constant, then any contribution of Marangoni stresses to the dynamics from Equation (37) is eliminated. Then we can neglect surfactant transport and we have the two coupled equations (35) and (36), the equations for the surface velocity $w^{(S)}$ and the evolution of the interface shape k, respectively. In later parts of this paper, we shall designate this limit with the shorthand $\mathcal{M} = 0$.

Free-surface shapes at time $t = 16$, for several values of $\mathcal{S}$ in the range 10^2 to 10^6 with $k_z(L, t) = 10$ are plotted in Figure 3. As $\mathcal{S}$ decreases, drainage is much faster and the film thins more rapidly; free-surface shapes for smaller $\mathcal{S}$ take on the typical concave-out shapes for mobile films given in Chapter IV of Mysels *et al.* [1].

In Figure 4, comparison of $w^{(S)}$ is made for different values of $\mathcal{S}$ ranging between $10^6 - 10^2$ at $t = 16$. For large $\mathcal{S}$, $w^{(S)}$ is almost zero, and the film is practically immobile. As $\mathcal{S}$

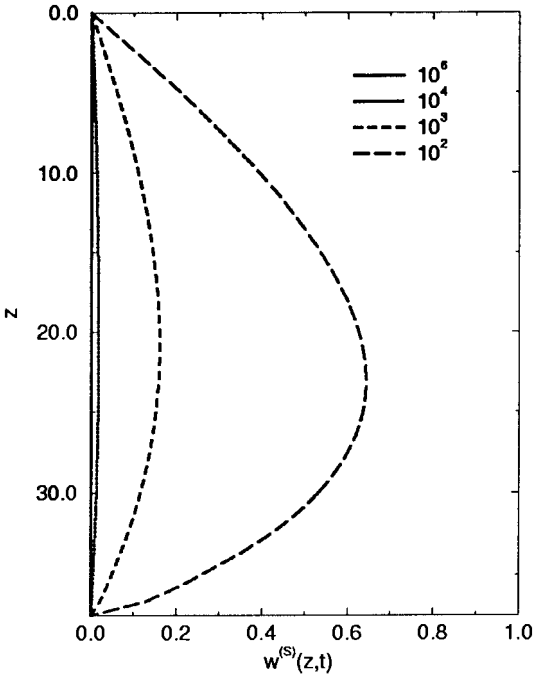

Figure 4. $w^{(S)}$ at $t = 16$ for several $\mathcal{S}$ (upper right). The flow is much faster for small values of $\mathcal{S}$ and becomes practically zero for large values of $\mathcal{S}$.

decreases; the flow along the surface is much faster; this makes the free surface more mobile, which makes the film thin faster.

Further results along this line are given in [29]. We note that this is only one way to span the behavior from mobile to rigid-surface behavior. The Marangoni effect can also make the film surface rigid, and we report results on this next.

3.2.2. *Constant surface viscosity and Marangoni effects*

We now consider the case where the Marangoni effect and surfactant transport is included in the model. The tangential shear stress includes the stress due to the change of surface tension in the presence of concentration gradients, and so Marangoni effects are included.

The initial conditions are as before for k and $w^{(s)}$; for the concentration we have

$$\Gamma(z, 0) = \frac{1 + \tanh(z - L + 2)}{2}. \tag{56}$$

For this kind of initial condition the problem bears some resemblance to the surfactant-spreading problem [63]. We have also studied the case with a linear initial profile for the surfactant distribution [31]; there is no qualitative difference in the results.

Marangoni effects have a substantial impact for smaller values of $\mathcal{S}$, retarding surface drainage and increasing film thickness; free-surface shapes for varying $\mathcal{M}$, with $\mathcal{S} = 10^2$, $\mathcal{P} = 10^2$ and $t = 32$ are shown in Figure 5. For small $\mathcal{M}$, surface-tension gradients are too weak to retard drainage and the film thins rapidly. As $\mathcal{M}$ increases, surface-tension gradients become more prominent and transistion from a mobile to an essentially immobile film is observed ($\mathcal{M} = 10^2$). As $\mathcal{M} \to \infty$, $w^{(S)}$ goes to zero and the surface becomes rigid. Figure 6 plots the surface velocity, $w^{(S)}$, at $t = 32$ for varying $\mathcal{M}$ with $\mathcal{S} = 10^2$ and $\mathcal{P} = 10^2$. For

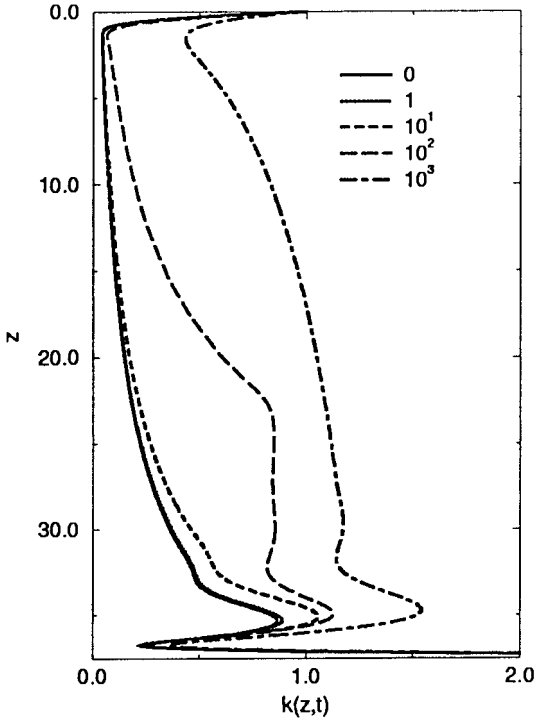

Figure 5. Film shape at $t = 32$ with $\mathcal{S} = 10^2$ and $\mathcal{P} = 10^2$ for several values of $\mathcal{M}$ (shown in the upper right). The film in much thinner for small values of $\mathcal{M}$ (surface tension gradients negligible). For large values of $\mathcal{M}$, Marangoni effects are stronger, drainage is retarded and the free surface becomes immobile.

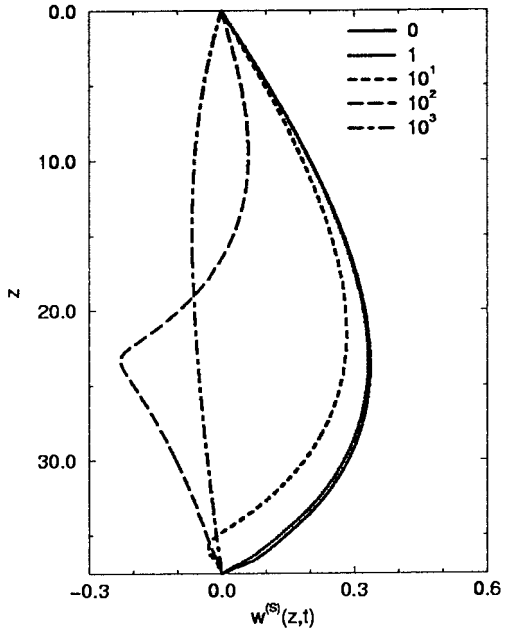

Figure 6. $w^{(S)}$ at $t = 32$ with $\mathcal{S} = 10^2$ and $\mathcal{P} = 10^2$ for several values of $\mathcal{M}$ (shown in the upper right). For large values of $\mathcal{M}$, Marangoni effects are strong enough to cause flow reversal, *i.e.*, Marangoni flow, enhancing film thickness. For smaller values of $\mathcal{M}$, Marangoni effects are too weak to retard drainage and the film thins rapidly.

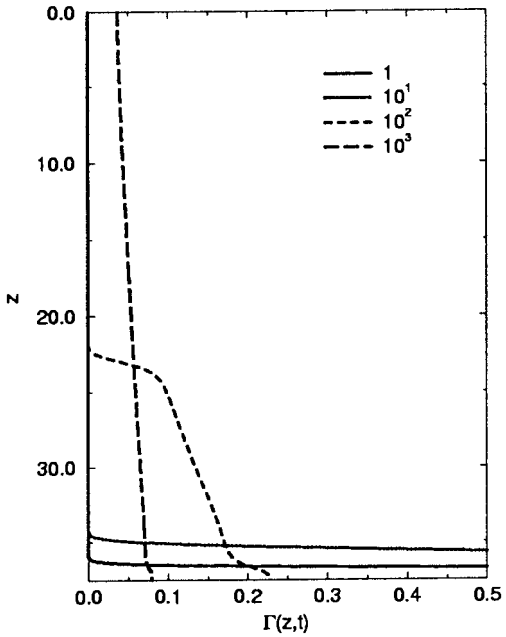

Figure 7. Γ at $t = 32$ with $\mathcal{S} = 10^2$ and $\mathcal{P} = 10^2$ for several values of $\mathcal{M}$ (shown in the upper right). For large values of $\mathcal{M}$, Marangoni flow is strong enough to drag the surfactant up the film. For smaller values of $\mathcal{M}$, $w^{(S)}$ is large and the surfactant is swept to the bottom of the film.

large values of $\mathcal{M}$, Marangoni effects are strong enough to cause the flow to reverse , *i.e.*, $w^{(S)} < 0$, retarding drainage and enhancing film thickness (Figure 5). For smaller values of $\mathcal{M}$, the Marangoni effect is too weak to retard drainage and the film thins rapidly. Figure 7 shows the surfactant concentration, $\Gamma(z, t)$, at $t = 32$ for several values of $\mathcal{M}$ with $\mathcal{S} = 10^2$ and $\mathcal{P} = 10^2$. For large values of $\mathcal{M}$, the Marangoni effect is strong enough to drag the surfactant up the film. For smaller values of $\mathcal{M}$, $w^{(S)}$ is large and the surfactant is swept to the bottom of the film.

We now discuss the time evolution and power-law behavior of k. For very large $\mathcal{M}$, we find that the exponent of the film thickness tends to be a power-law with $t^{-0{\cdot}5}$, which is the rigid limit. For smaller $\mathcal{M}$, we find that the thinning of the film tends to roughly $t^{-0{\cdot}9}$, which is the mobile limit. For $\mathcal{M} = 10^2$ we have computed the exponent at the elevations $z = 10$, $z = 18{\cdot}75$ and $z = 25$ which are representative of the top, middle and bottom portions of the film. At $z = 10$, for early times, the top portion of the film is essentially mobile. At later times, the decay of the thickness tends to about $t^{-0{\cdot}6}$ behavior at all three locations; this implies that the film has become approximately rigid. This depicts the transistion from a mobile to an essentially immobile behavior as seen in Figure 5. Snow *et al.* [21, 64] have observed intermediate power-law behavior within the range $-0{\cdot}7$ to $-0{\cdot}8$. Based on a variety of calculations (not shown), our intermediate power law exponents lie between $-0{\cdot}5$ and $-0{\cdot}6$.

3.3. NONLINEAR SURFACE PROPERTIES

We now compute solutions to the model derived in the formulation section of the paper where both the surface tension and surface viscosity depend nonlinearly on the surfactant concentration.

The initial conditions are as in the previous section except that we have imposed the linear initial concentration profile as described in Section 3. These initial conditions are a convenient choice and did not affect the long-time behavior of the film in prior papers [28, 29, 39]. However, for the results of this section, there may be cases where the evolution is rapid enough that this no longer is true.

Figures 8–10 plot k, $w^{(S)}$ and Γ, respectively, as functions of t. The parameter values used for this case are as follows:

$$\mathcal{S} = 30, \quad \mathcal{M} = 10^3, \quad \mathcal{P} = 10^4, \quad \alpha = -6{\cdot}2, \quad \alpha_1 = 1{\cdot}0, \quad g_0 = 0{\cdot}5 \quad g_1 = 0{\cdot}7.$$

$\mathcal{S}G$ ranges approximately between 1–50 and $\mathcal{M}F_\Gamma$ is roughly between 500–1000 for Γ varying between 0·01–0·9. Near the top of the film the Marangoni effects and the surface viscous effects are not as large compared to the middle and the bottom. This low shear from surface viscous and Marangoni effects causes rapid downward surface flow (see Figure 9) and the film thins rapidly near the top (see Figure 8). This rapid drainage sweeps all the surfactant near the top to the middle and lower regions of the film (see Figure 10). This enhances both the Marangoni and the surface viscous effects in the middle of the film. Significant shear stresses are generated and this causes the surface flow to reverse (see Figure 9). This flow reversal drags the surfactant up the film which drives the travelling surfactant front (see Figure 8) to the top of the film. This front, like the constant surface viscosity case, is also approximately rigid behind it and mobile in front of it.

Note that all of the concentration variation is now confined near the top of the film, and this localization has minimized the impact of the conditions used at the bottom of the film. This sort of localization does not occur for the case with linearized properties studied in the previous section.

4. Results without mean surface tension

We now turn to investigating how much of the film drainage behavior can be deduced without having do deal with the ends of the film. In order to do this, we must study the approximation which governs the long, relatively flat, middle region of the film. In this region, we develop a simpler model which can still capture a mobile-to-rigid transition. We begin by seeing the reduction in the tangentially immobile case, and then move on to include mobile surfaces.

4.1. TANGENTIALLY IMMOBILE CASE

One can rescale Equation (47) with $z = Z/\delta$, $t = T/\delta$ and $k(z, t) = K(Z, T)$ with Z and T both $O(1)$, to arrive at a model which does not include the high derivatives associated with surface tension at leading order in δ [28]. This model approximates the long middle region of the film between the meniscus at the top and the capillary wave at the bottom. One obtains

$$K_T + K^2 K_Z = 0, \tag{57}$$

which is a well-known nonlinear wave equation [62, Chapter 2] and has arisen in a variety of contexts (*e.g.*, [5]). A solution to Equation (57) is given implicity by

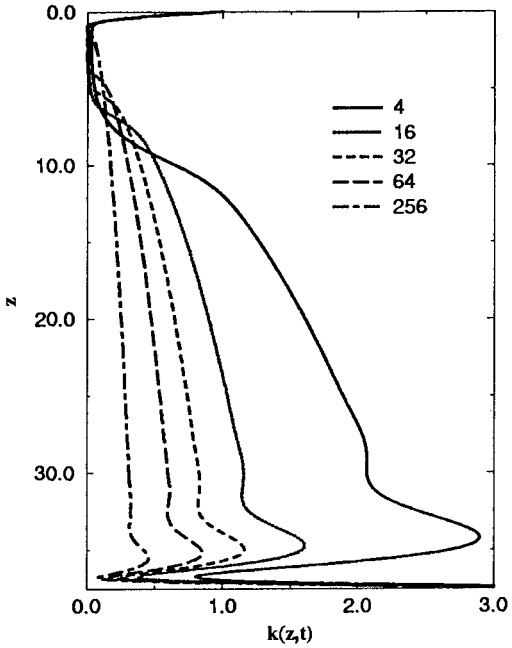

Figure 8. $k(z,t)$ for several t (upper right). The travelling front seen in the top portion goes all the way to the top of the film. The surfactant front is again driven by shear stresses from surface-tension gradients which gradually build up from the middle and lower regions of the film (there is also considerable shear from the surface viscous effects for this case).

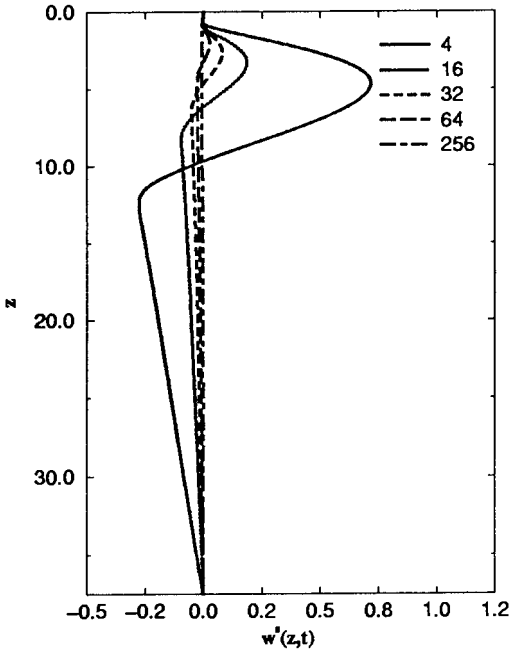

Figure 9. $w^{(S)}(z,t)$ for several t (upper right). The predominately downward surface flow near the top sweeps that region almost clean of surfactant and increases the concentration in the middle and lower regions of the film. The resulting shear from surface-tension gradients and the surface viscous effects cause flow reversal; this in turn drags the surfactant up the film helping to drive the travelling surfactant front seen in Figure 8.

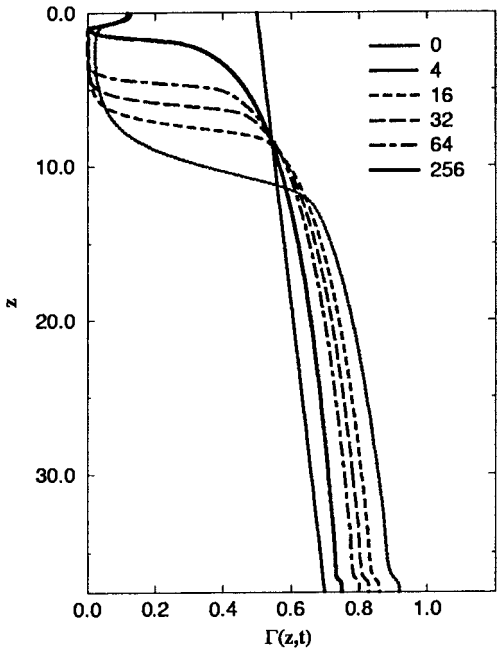

Figure 10. $\Gamma(z, t)$ for several t (upper right). The downward surface flow near the top of the film sweeps that region almost clean of surfactant and increases the concentration near the middle and lower regions of the film. Significant shear from surface-tension gradients and also surface viscous effects occur in the middle and lower regions causing the film to thicken and the flow to reverse. As time increases, the reverse flow drags the surfactant up the film helping to drive a travelling front seen near the top (see Figure 8).

$$K(Z, T) = K_0(\, Z - T K^2(Z, T)\,). \tag{58}$$

Here $K_0(Z) \equiv K(Z, 0)$ is the initial profile of the film. The solution says that the speed of a given thickness of the initial profile is proportional to the square of the thickness. For an initial profile that has positive slope everywhere, the higher parts move faster than the lower parts but no shocks form. For a linear initial condition and for $T \gg 1$ and Z bounded away from the origin [28], we find to leading order that $K \sim \sqrt{Z/T}$. This agrees with the analysis Mysels *et al*. [1] and an analysis by Pernisz [61], and it gives the thinning rate for the film in the slow draining limit from this drastically simplified model. It is also worth noting that the linear initial condition is a convenient choice and still gives results that are relevant to the experimental results for longer times [22].

A similar approach can be applied to the more general model with constant surface viscosity and a linearized surface viscosity. We call the resulting equations the 'flat film' model. We will first consider only surface viscous effects, neglecting Marangoni effects. This could correspond to a high concentration of surfactant uniformly distributed along the free surface. Then we will consider both surface viscous and Marangoni effects.

4.2. Mobile flat-film model

We now consider the case where the film is mobile. The surface can now advect surfactant and modify the concentration field. The tangential shear stress includes the stress due to the change of surface tension in the presence of concentration gradients, and so Marangoni effects are included.

Rescaling Equations (35)–(37) with

$$z = \frac{Z}{\delta}, \quad t = \frac{T}{\delta}, \quad \bar{\mathcal{S}} = \frac{\mathcal{S}}{\delta^2} \quad \text{and} \quad \bar{\mathcal{M}} = \frac{\mathcal{M}}{\delta}, \tag{59}$$

where T, Z, $\bar{\mathcal{S}}$ and $\bar{\mathcal{M}}$ are $O(1)$, $k(z,t) = K(Z,T)$, $w^{(S)}(z,t) = W^{(S)}(Z,T)$ and $\Gamma(Z,T) = \Gamma(z,t)$; we arrive at

$$K_T + \left[K W^{(S)} + \frac{K^3}{3} \right]_Z = 0, \tag{60}$$

$$\bar{\mathcal{S}} W^{(S)}_{ZZ} + K + \bar{\mathcal{M}} \Gamma_Z = 0, \tag{61}$$

$$\Gamma_T + \left[\Gamma W^{(S)} \right]_Z = 0. \tag{62}$$

Here we have also let $\mathcal{P} \to \infty$ to eliminate surface diffusion from the problem.

The boundary conditions are given by

$$K(0,T) = W^{(S)}(0,T) = \Gamma(0,T) = W^{(S)}_Z(L,T) = 0. \tag{63}$$

where L is specified as data, and results are computed for a given value.

This choice of the boundary condition for K at $Z = 0$ can be motivated by considering this problem without surface tension as an 'outer' approximation to the meniscus that is developing close to the wire frame where surface tension is important [28]. The dynamic behavior of the film thickness in this region is $K \to 0$ for long times. For a tangentially-immobile film, Braun *et al*. [28, 33] have shown that this approximation is in good agreement with the problem including surface tension and gets better with increasing time.

The boundary condition for $W^{(S)}$ at $Z = L$ can be determined by looking at the results from the whole film. At the top where the film connects to the wire frame, $W^{(S)} = 0$; at the bottom where the film connects to the static meniscus, $W^{(S)}$ should also equal zero. Hence, $W^{(S)}$ attains its maximum somewhere within the film and that is taken as the end of the computational domain, $Z = L$ (say), in our model. The initial condition for K is

$$K = K_0(Z). \tag{64}$$

The initial conditions specified for K and Γ are

$$K(Z,0) \equiv K_0(Z) = S_1 Z \tag{65}$$

and

$$\Gamma(Z,0) \equiv \Gamma_0(Z) = g_0 + (g_1 - g_0)\frac{Z}{L}. \tag{66}$$

Here g_0 and g_1, is the surfactant concentration at $Z = 0$ and $Z = L$, respectively. For all results presented below, we will have $S_1 = 0{\cdot}23$ and $L = 20$. The length of the domain reflects the fact that the equations are now on the scale of the static meniscus radius and that the film must be at least a few times this length in order for the results to be valid.

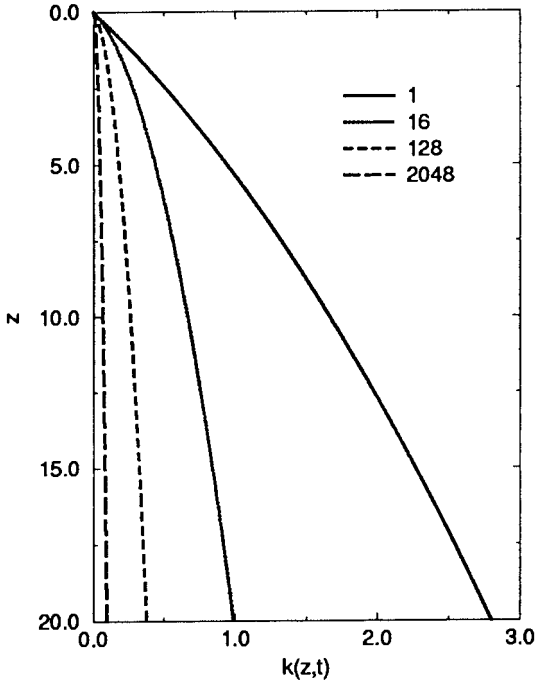

Figure 11. Film shape with $\bar{\mathcal{S}} = 10^6$ for several values of T (shown in the upper right). The initial film is $K_0 = 0{\cdot}23Z$, the film thins and becomes parabolic as time progresses. Free surface shapes match extremely well to those obtained using large $\bar{\mathcal{S}}$ asymptotics (see Section 4.2.3).

4.2.1. *Results with* $\bar{\mathcal{M}} = 0$

In this limit, the evolution of the surface concentration decouples from the problem, and need not be considered. For our choice of initial conditions and $\bar{\mathcal{M}} = 0$, we have $W^{(S)}(Z, 0) = S_1 Z(L^2 - Z^2/3)/(2\bar{\mathcal{S}})$.

Free-surface shapes as a function of time for $\bar{\mathcal{S}} = 10^6$ and $\bar{\mathcal{M}} = 0$ are shown in Figure 11. The initially-linear film thins and becomes parabolic in shape as time progresses. This type of free-surface shape agrees well with the results from the tangentially-immobile case [28, 33]. In the limit of $\bar{\mathcal{S}} \to \infty$, the free-surface shape tends asymptotically to that of a tangentially-immobile film; this is discussed in more detail in [39]. The downward parabolic shape agrees with the typical rigid film profiles given in Chapter III of Mysels *et al*. [1].

Lowering the value of $\bar{\mathcal{S}}$ in this model is a way for the surface to remobilize and speed up the film drainage. Free-surface shapes at time $T = 16$, for several values of $\bar{\mathcal{S}}$ in the range 1 to 10^6, are plotted in Figure 12. The shapes for smaller $\bar{\mathcal{S}}$ take on the typical shapes for mobile films given in Chapter IV of Mysels *et al*. [1], which they described as 'hollow ground.'

In Figure 13, comparison of $W^{(S)}$ is made for different values of $\bar{\mathcal{S}}$ at $T = 16$. The flow along the surface is much faster as $\bar{\mathcal{S}}$ decreases; this makes the free surface more mobile, which makes it thin faster.

4.2.2. *Results with* $\bar{\mathcal{M}} \neq 0$

The nonlinear coupled PDEs, (60), (61) and (62), are again written in the form of a differential-algebraic system as done in Section 4.2.1 and solved using initial conditions $K_0(Z) = S_1 Z$ and $\Gamma_0(Z) = Z/L$, with S_1 and L as defined before. An initial linear surfactant concentration profile is again a convenient choice and this does not affect the long-time behavior of the film.

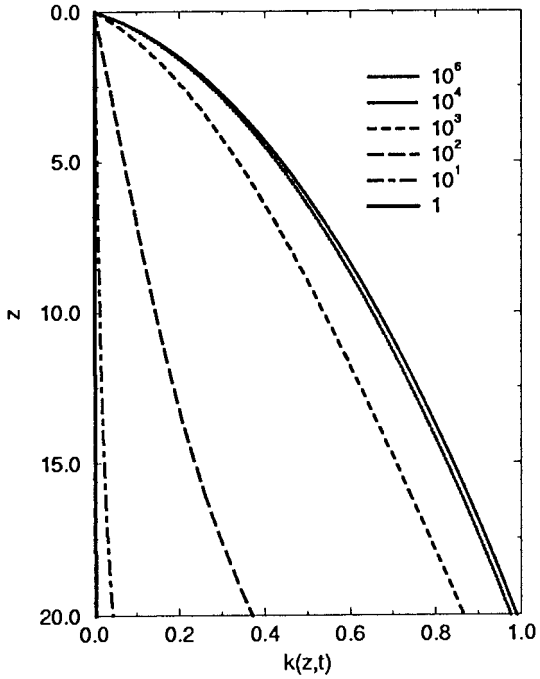

Figure 12. Film shape at $T = 16$ for several values of $\bar{s}$ (shown in the upper right). The film in much thinner for small values of $\bar{s}$ because the free surface is mobile. For large values of $\bar{s}$, the free surface becomes practically immobile and stability of the film is greatly enhanced.

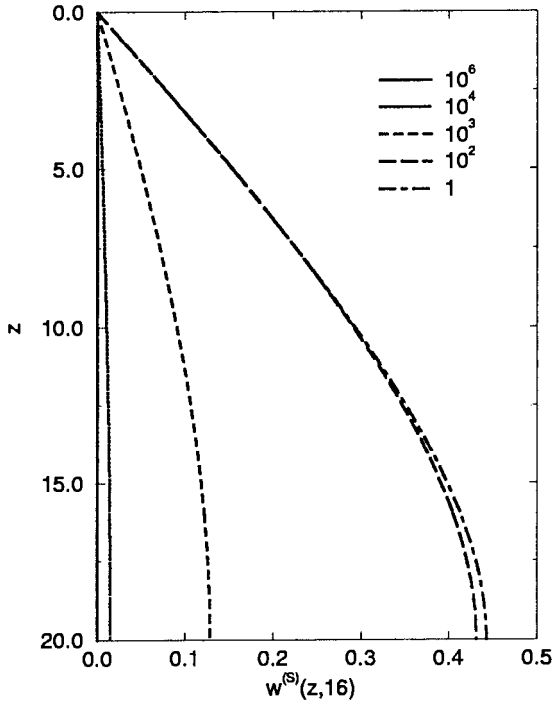

Figure 13. $W^{(S)}$ at $T = 16$ for several values of $\bar{s}$. Surface velocity becomes appreciable for small $\bar{s}$, the film is more mobile and thins rapidly.

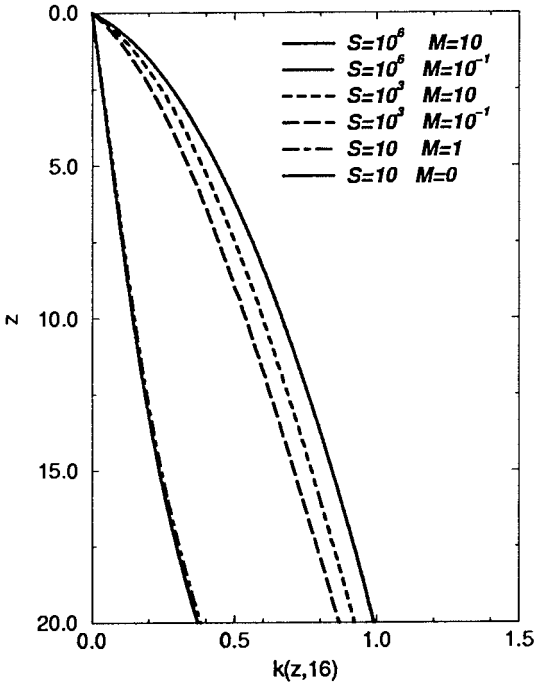

Figure 14. Film shapes at $T = 16$ for several $\bar{\mathcal{S}}$ and $\bar{\mathcal{M}}$ (shown upper right). Concentration gradient effects are insignificant for $\bar{\mathcal{S}} = 10^6$ hence the film shapes are indistinguishable for different $\bar{\mathcal{M}}$ (rightmost curve). A significant increase in film thickness is observed for the intermediate value of $\bar{\mathcal{S}} = 10^3$, where concentration gradients play a significant role (middle curves). For $\bar{\mathcal{S}} = 10^2$ (and smaller), the film is slightly thicker for larger $\bar{\mathcal{M}}$ due to weak concentration-gradient effects (leftmost curves).

In Figure 14, film shapes at time $T = 16$ are shown for various $\bar{\mathcal{S}}$ and $\bar{\mathcal{M}}$. For $\bar{\mathcal{S}} = 10^3$, the film is significantly thicker for $\bar{\mathcal{M}} = 10$ than for $\bar{\mathcal{M}} = 10^{-1}$. For $\bar{\mathcal{S}} = 10^2$, the film is slightly thicker close to the bottom ($Z = L$) for $\bar{\mathcal{M}} = 1$ than for $\bar{\mathcal{M}} = 0$. As the film gets more mobile, interfacial concentration gradients significantly affect the flow, and weakly affects the free-surface shapes. Marangoni effects have a negligible effect on $W^{(S)}$ at a large value of $\bar{\mathcal{S}}$, *e.g.*, $\bar{\mathcal{S}} = 10^6$. Figure 15 plots the surface velocity at $T = 16$ for varying $\bar{\mathcal{S}}$ and $\bar{\mathcal{M}}$. For $\bar{\mathcal{S}} = 10^3$, the flow is slower for $\bar{\mathcal{M}} = 10$ than for $\bar{\mathcal{M}} = 1$; this is due to Marangoni effects. For $\bar{\mathcal{S}} = 10^2$ there is no appreciable change in the surface velocity. This indicates that Marangoni effects are more prominent at some intermediate values of $\bar{\mathcal{S}}$ and $\bar{\mathcal{M}}$ in this model. Figure 16 shows the surfactant concentration at $T = 16$ for several values of $\bar{\mathcal{S}}$ and $\bar{\mathcal{M}}$. There is a marked change in the surfactant concentration profiles as $\bar{\mathcal{S}}$ decreases. This change is due to increasing $W^{(S)}$ as $\bar{\mathcal{S}}$ decreases; the increasing surface velocity sweeps out more surfactant.

This model suffers from the limitation that the Marangoni effect must be relatively weak for the above-specified problem to hold. If the Marangoni effect is too strong, fluid may enter the film from the bottom, and the boundary conditions given above may not be used. For more detail, see [39].

We now discuss the time evolution and power-law behavior of K. In the flat-film model only, $\bar{\mathcal{M}}$ must remain small and thus plays no role in the limiting cases of the drainage. For very large $\bar{\mathcal{S}}$, we find the exponent of the film thickness tends to a power law that decays like $T^{-0{\cdot}5}$; for smaller $\bar{\mathcal{S}}$, we find the thickness decreases like T^{-1}. The large $\bar{\mathcal{S}}$ value agrees very

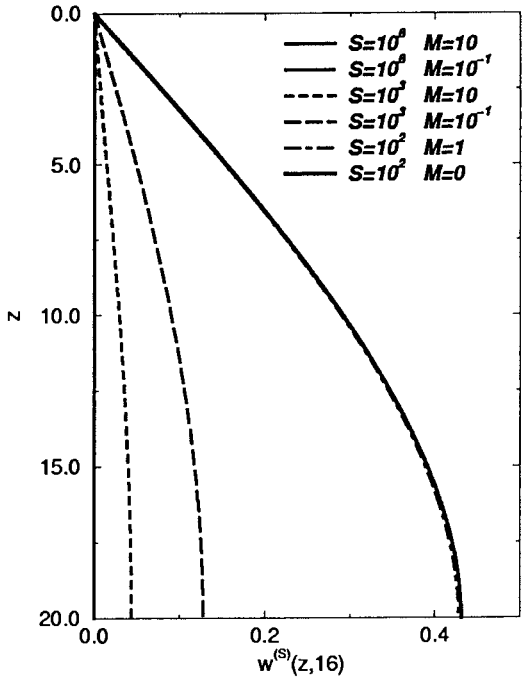

Figure 15. $W^{(S)}$ at $T = 16$ for several $\bar{\mathcal{S}}$, with $\bar{\mathcal{M}}$ given in the upper right. The Marangoni effect is insignificant for large $\bar{\mathcal{S}}$ because $W^{(S)}$ is indistinguishable for different values of $\bar{\mathcal{M}}$; the left edge of the plot is two superimposed curves. For $\bar{\mathcal{S}} = 10^3$ we see that the flow slows down significantly, causing a significant increase in film thickness (see Figure 14). As $\bar{\mathcal{S}}$ decreases, there is a slight decrease in surface velocity contributing to a weak thickening in the film shape (rightmost curves).

well with the tangentially-immobile case [28, 33]. The smaller $\bar{\mathcal{S}}$ value is again consistent with faster drainage.

These exponent values are very close to experimental values obtained by Snow *et al*. [21], *i.e.* $-0{\cdot}47$ and $-0{\cdot}92$ for their most rigid and mobile films, respectively. This agreement with the range of values of the experimental thinning rates provides strong support for this modeling approach.

4.2.3. *Asymptotic results: large and small* $\mathcal{S}$

We have also studied the limiting cases of large and small $\bar{\mathcal{S}}$ using perturbation methods. For $\bar{\mathcal{S}} \gg 1$, the analysis shows how to obtain the $T^{-1/2}$ thinning for these nearly-tangentially-immobile films. The leading-order surface velocity is zero and the leading-order surfactant concentration is constant; corrections to these quantities may be found analytically. For $\bar{\mathcal{S}} \ll 1$, the analysis gives similarity behavior for the T^{-1} thinning rate, and a boundary-value problem to solve (numerically) to obtain the surface shape, velocity and concentration. Details of these analyses can be found in [39].

4.2.4. *A connection with extensional flow*

For the case when $\bar{\mathcal{S}} \ll 1$, we can show an overlap in the behavior that occurs in the long-time behavior. We postulate an intermediate regime where both extensional and shear-flow components contribute equally to the dynamics of the problem. Use the decomposition

$$w(x, z, t) = w_1(x, z, t) + w^{(S)}(z, t), \tag{67}$$

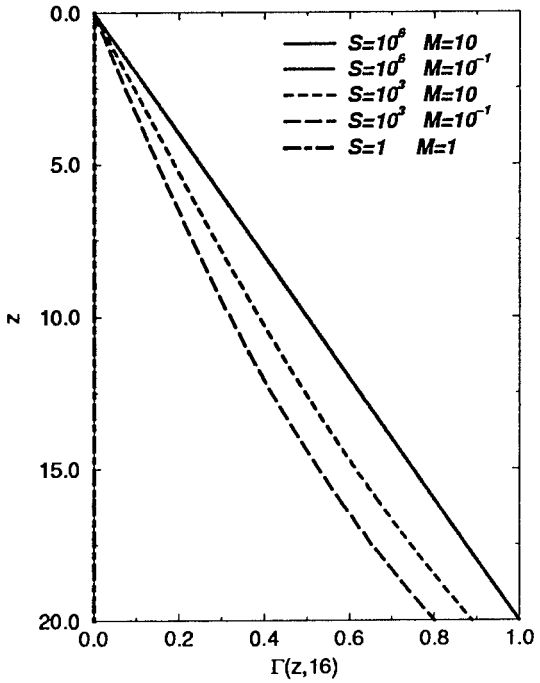

Figure 16. $\Gamma(Z, 16)$ for several $\bar{\mathcal{S}}$ and $\bar{\mathcal{M}}$ as shown in the upper right. For large $\bar{\mathcal{S}}$, $W^{(S)}$ is small and Γ remains unchanged. As $\bar{\mathcal{S}}$ decreases, $W^{(S)}$ increases and the Γ profile is strongly affected. There is a significant difference in concentration profiles for $\bar{\mathcal{S}} = 10^3$.

where w_1 is the shear component that satisfies the no-slip condition on the free surface and $w^{(S)}(z, t)$ is the extensional component (as, for instance, in [57, 55, 32]). In order for these two contributions to have a comparable effect, the required physical balance must be $w^{(S)}_{zz} \sim w_{1xx}$. The velocity scales are thus related according to

$$W^{(S)} = \frac{W}{\delta^4}, \tag{68}$$

for the extensional (or slug-flow) scale $W^{(S)}$ and the sheared part the velocity scales with W as defined in Equation (13). The following rescalings are also appropriate:

$$\tilde{u} = \delta^4 u, \quad \tilde{t} = \frac{t}{\delta^4}, \quad \tilde{\Gamma} = \delta^4 \Gamma, \quad \tilde{\mathcal{S}} = \frac{\bar{\mathcal{S}}}{\delta^4}, \quad \tilde{\mathcal{M}} = \frac{\bar{\mathcal{M}}}{\delta^4}, \quad \tilde{\mathcal{P}} = \frac{\bar{\mathcal{P}}}{\delta^4}, \tag{69}$$

Substituting these rescalings, together with Equations (67) and (68), in Equations (16)–(23) gives the following leading-order problem in the film

$$\tilde{u}_{\tilde{x}} + \tilde{w}^{(S)}_{\tilde{z}} = 0, \tag{70}$$

$$0 = -\tilde{p}_{\tilde{x}} + \tilde{u}_{\tilde{x}\tilde{x}}, \tag{71}$$

$$0 = -\tilde{p}_{\tilde{z}} + \tilde{w}^{(S)}_{\tilde{z}\tilde{z}} + \tilde{w}_{1\tilde{x}\tilde{x}} + 1. \tag{72}$$

These are subject to the symmetry condition at $\tilde{x} = 0$,

$$\tilde{u} = \tilde{w}_{1\tilde{x}} = 0. \tag{73}$$

At $\tilde{x} = \tilde{k}(\tilde{z}, \tilde{t})$ we have

$$\tilde{k}_{\tilde{z}\tilde{z}} = -\tilde{p} + 2\tilde{u}_{\tilde{x}}, \tag{74}$$

$$\tilde{\mathcal{M}}\tilde{\Gamma}_{\tilde{z}} + \tilde{\mathcal{S}}\tilde{w}^{(S)}_{\tilde{z}\tilde{z}} = 2\tilde{k}_{\tilde{z}}(\tilde{u}_{\tilde{x}} - \tilde{w}^{(S)}_{\tilde{z}}) + (\tilde{u}_{\tilde{z}} + \tilde{w}_{1\tilde{x}}), \tag{75}$$

$$\tilde{k}_{\tilde{t}} - \tilde{u} + \tilde{k}_{\tilde{z}}\tilde{w}^{(S)} = 0. \tag{76}$$

Using a similar procedure as in Section 4.2 and neglecting average surface tension effects, we obtain the rescaled flat-film equations

$$\tilde{\mathcal{S}}\tilde{w}^{(S)}_{\tilde{z}\tilde{z}} + 4\left(\tilde{k}\tilde{w}^{(S)}_{\tilde{z}}\right)_{\tilde{z}} + \tilde{k} + \tilde{\mathcal{M}}\tilde{\Gamma}_{\tilde{z}} = 0, \tag{77}$$

$$\tilde{k}_{\tilde{t}} + \left(\tilde{k}\tilde{w}^{(S)}\right)_{\tilde{z}} = 0, \tag{78}$$

$$\tilde{\Gamma}_{\tilde{t}} + \left(\tilde{\Gamma}\tilde{w}^{(S)}\right)_{\tilde{z}} - \frac{1}{\tilde{\mathcal{P}}}\tilde{\Gamma}_{\tilde{z}\tilde{z}} = 0. \tag{79}$$

When compared to Equations (60)–(62), the extensional term now appears in the tangential-stress balance (alternatively, the equation for the surface velocity), while the gravitational term in Equation (78) for $\tilde{k}$ does not. However, one can again seek solutions as an expansion in powers of $\tilde{t}^{-1}$ as described above. The terms that contribute at leading order in the Equations (77)–(79) are precisely the common terms with the flat-film formulation of Section 4. Hence, at long times, one would expect the same leading-order behavior from either of the regimes we have given, namely one which includes extensional-flow effects or not.

5. Discussion

5.1. Our work

We have presented models for vertical film drainage that span the range from mobile to rigid behavior. The transition from mobile to rigid behavior could occur via either strong surface viscous or strong Marangoni effects. While the rigidification of a free surface has been calculated via Marangoni effects (*e.g.*, [32, 34, 38]), we consider it a strength of our model that we can include surface viscosity and study its interplay with other effects.

Our work has studied in detail the different regions of the film that develop during the evolution. The development of the different regions has allowed quantitative study of the different roles they play and the dominance of different physical effects in each. The interchange of different dominant balances in the bumps and dips above the bath have been studied in [28]; each bump and dip has a different balance and a different exponent for thinning. The long flat middle region may profitably be studied by scaling the lengths and times to eliminate the contribution of mean surface tension [39]. This approach illustrates the roles of minimal sets of physical effects necessary to achieve the fast and slow draining behavior in vertical films. The roles of nonlinear surface properties as opposed to a linearized approximation to surface properties has also been investigated [29], with localization occuring in the cases with nonlinear properties [30] that may be necessary for the complex behavior observed experimentally in the transition zone [1, 21, 26].

The results show a film composed of several regions; moving vertically downward, we find an upper meniscus, a long 'flat' middle, bumps and dips, and finally a static meniscus region. The bumps and dips (or capillary wave) end in the transition region between the thin film and the bath (where the static meniscus region is assumed). The static meniscus region has been taken to be analogous to a Plateau border region. While this analogy and film structure works well for the rigid case, the mobile case may be more difficult for making comparisons. For a mobile film draining horizontally into a Plateau border, the sequence of bumps and dips may be absent [24, 25]. This may be a result of the absence of a gravitational effect in the horizontal drainage. The bottom of the images in Figure 1 in [23] would be a direct comparison with theory of this paper, but the transition region at the bottom of their film is not investigated closely enough for comparsion. We do not believe that was the intention of the investigation in [23] in any case; their intent was to investigate marginal regeneration on the vertical sides of the film. We also note that in the study of Breward [17, Chapter 5], there could be either monotonic or nonmonotonic profiles for the film connecting to the Plateau border in the absence of gravity, depending on the conditions of the analysis.

We are now in a position to make a closer comparison with the work of Nierstrasz and Frens [27]. They developed evolution equations for surface velocity, film thickness, and surface and bulk concentrations. They find concentration gradients in the transition zone between the thin film and a Plateau border region in the bottom of the film. The film comprises about one quarter of the computational domain in their work, whereas in our work the film occupies the vast majority of the computational domain. In the Plateau border, Neirstrasz and Frens appear to abandon the conservation equation for solute inside the film and enforce a constant concentration in this region (second paragraph in Results section); we believe this is the source of the rapid change in the dependent variables and that this is the reason that the concentration gradient in the transition region appears to be stuck there (unable to move with the surface velocity it generates). In our model, concentration gradients also generate a surface velocity, but they can interact and the concentration gradient is free to be advected within the transition zone and film. While a soluble surfactant is considered in [27], the mathematical implementation with a connection to the Plateau border at the bottom of the film appears to be problematic.

5.2. Opportunities

5.2.1. *Extensional flow regimes*

This work is based on the scaling of the tangentially immobile film. Many practical situations have a mobile surface, and the film, in some situations, may be closer to an extensional flow. Work which approaches the problem from that viewpoint may be successful in some parameter ranges where our approach would fail. Schwartz and Roy [32] studied a vertical film entirely within a frame, and their scalings come from an extensional flow limit. They capture both rigid and mobile behavior, and observed the formation of thin regions that they interpreted as the beginnings of a black film. Breward [17, Chapter 5] also investigates extensional flow effects of film drainage into a lamella. We have shown above that similarity behavior at long times in the mobile case for our model gives the same T^{-1} behavior as an extensional flow model; in other situations it may be necessary to include extensional flow terms.

5.2.2. *Computing flow in both the film and the bath*
The results presented here use an asymptotic patch to connect the thin film (governed by lubrication equations) with the hypothesized static meniscus (that approximates the bath). This assumption has lead to increased understanding, but it would be satisfying to tie together the draining film and the bath in a more versatile manner. Hansen [65] has studied the steady flow of a film into a bath for a pure liquid with no shear stress on the free surface using boundary-integral methods. Kheshgi *et al*. [51] have also studied a variety of conditions for terminating a film for coating processes. For a recent review of related models in coating flows, see [66]. The current situation would require one to generalize to include surfactant transport and a dynamic flow.

5.2.3. *Soluble surfactants*
Most films have a soluble surfactant present; we have only treated insoluble surfactants to date, but other authors have included soluble surfactants in their models (*e.g.*, [17, Chapter 5], [27]). The soluble surfactant would require the solution of a PDE inside the film for the concentration of the surfactant as some additional terms to govern the exchange of surfactant between the surface and the inside of the film. The approximation we have used with an asymptotic patch to a static meniscus is clearly not sufficient to treat this case, and the flow in the bath must be computed in concert with the film flow. This is an active area of research.

5.2.4. *Three-dimensional model*
We have computed a solution to a problem for the vertical film with constant surface viscosity, surfactant transport, and the Marangoni effect [67]. An instability occurs because of the competition between gravitational and Marangoni effects; gravity causes drainage, but the drainage increases the concentration gradients near the bottom of the film. These forces cause a recirculation on the surface. Such an instability was found in the closely related problem of the drainage of a film in a horizontal ring by Joye and coworkers [14, 15]; they were the first to compute this kind of solution. Bruinsma [16] studied the analogous problem using a quasisteady approximation for a base state with equal surface viscosities to develop a stability theory for the vertical film case. He computed the stability boundary to within a constant multiple, and concluded that films would usually be unstable to a circulatory flow located around the transition region. He did expect to find downflow in thickened regions and upflow in thinned regions, as was observed in the numerics of Naire *et al*. [67].

In our work, the results were computed on a domain that was horizontally periodic; it would certainly be worthwhile to consider the case with a finite-width film.

While the instability is interesting, and there are special cases where it may be observed experimentally [22], the more common observation (particularly in aqueous systems) is that of ‘peacock feathers’ where there are thin finger-like structures moving up the film out of the region where the film connects to the bath [1, 21, 26]. No computed solutions have exhibited these dynamic structures to our knowledge. The main difficulty is that they have their origin precisely in the region where the scalings change from those of the thin film to those of the bath. This presents a computational and analytical challenge.

6. Conclusion

The overall goal of the project was to develop a physical model of a vertical, draining liquid film. This model would be used to compare to the results obtained from experiment. A sequence of models illustrates the roles played by the various effects. Initially, the film featured a free, but tangentially-immobile surface (infinite surface viscosity or strong Marangoni effect) which modeled the rigid films reported both in the literature and in the in-house experiments. Excellent agreement of theory with experiment was obtained regarding the fundamental parameter of the time exponent of drainage.

The next step was to relax the boundary condition of a tangentially-immobile surface, therefore allowing for a finite and variable surface viscosity and surfactant transport at the surface. The surfactant was fixed as being insoluble in the liquid phase (the 'insoluble monolayer' model). This model allowed for the capture of many of the features of the surface flows noted in the experiment and also the time exponent of drainage in the low-surface-viscosity regime. A key result is the description of the Marangoni effect as being the energetic driver of many of the surface flows. Also, it was shown that, at either high Marangoni number or high Boussinesq number, the drainage rate of the film could be severely retarded, at the extreme resulting in a rigid-surfaced film. This confirms ideas of many in the field of thin liquid films.

Finally, we have been able to acquire some results in the range of intermediate drainge rates, but they are only a limited part of the observed regimes. A number of new possible directions have been pointed out.

On the application side, our understanding of the behavior of silicone surfactants as stabilizers for polyurethane foams has tremendously increased. The model work has pointed the direction towards the development of new materials with elements of the holy grail in this field, the ability to predict the correlation of surfactant structure and concentration with foam performance. Operationally, we are much closer to being able to design a surfactant to yield specific foam performance. Fortunately this knowledge is also transferrable to the understanding and development of many dispersed physical and chemical systems, including emulsions and coating processes.

Acknowledgements

The authors gratefully acknowledge support from the National Science Foundation via Grants DMS-9620392, DMS-9631287 (RJB), DMS-9722854 (RJB,SN) and the Dow Corning Corporation (RJB, SN). The authors also thank U.C. Pernisz, A. Hirsa, J.M. Lopez and H.A. Stone for helpful conversations. RJB thanks the University of Southampton and EPSRC for support during completion of this work.

References

1. K.J. Mysels, K. Shinoda and S. Frankel, *Soap Films: Studies of their thinning and a Bibilography*, New York: Pergammon (1959) 116 pp.
2. D. Weaire and S. Hutzler, *The Physics of Foams*. Oxford: Oxford University Press (1999) 246 pp.
3. P.C. Hiemenz and R. Rajagopalan, *Principles of Colloid and Surface Chemistry*. New York: Marcel Dekker Inc. (1997) 650 pp.
4. D.T. Wasan, A.D. Nikolov, L.A. Lobo, K. Koceo and D.A. Edwards, Foalsn thin-films and surface rhestogical properties. *Progress in Surface Science* 39 (1992) 119–1189154.

5. A. Oron, , S.H. Davis and S.G. Bankoff, Long scale evolution of thin liquid films. *Rev. Modern Phys.* 69 (1997) 931–980.
6. I.B. Ivanov, and D.S. Dimitrov, Thin Film Drainage. In: I.B. Ivanov (ed.) *Thin Liquid Films*, Surfactant Science Series 29. New York: Dekker (1988) 379–495.
7. P.A. Kralchevsky, A.D. Nikolov, D.T. Wasan, and I.B. Ivanov, Formation and expasion of dark spots in stratifying foam films. *Langmuir* 6 (1990) 1180–1189.
8. D.A. Amos, J.H. Markels and C.J. Radke, Osmotic pressure and interparticle interaction in ionic micellar surfactant solutions. *J. Phys. Chem. B* 102 (1998) 2739–2753.
9. A.A. Sonin, A. Bonfillon and D. Langevin, The thinning of soap films: The role of surface viscoelasticity. *J. Colloid Interf. Sci.* 162 (1994) 323–330.
10. D.E. Tambe and M.M. Sharma, Hydrodynamics of thin liquid films bounded by viscoelastic interfaces. *J. Colloid Interf. Sci.* 147 (1990) 137–151.
11. L.W. Schwartz and H.M. Princen, A theory of extensional viscosity for flowing foams and concentrated emulsions. *J. Colloid Interf. Sci.* 118 (1987) 201–211.
12. A.M. Kraynik, Foam Flows. *Ann. Rev. Fluid Mech.* 20 (1988) 325–357.
13. E. Ruckinstein and A. Sharma, A new mechanism of film thinning: Enhancement of Reynold's velocity by surface waves. *J. Colloid Interf. Sci.* 119 (1987) 1–13.
14. J.L. Joye, G.J. Hirasaki and C.A. Miller, Asymmetric drainage in foam films. *Langmuir* 10 (1994) 3174–3179.
15. J.L. Joye, G.J. Hirasaki, and C.A. Miller, Numerical simulation of instability causing asymmetric drainage in foam films. *J. Colloid Interf. Sci.* 177 (1996) 542–552.
16. R. Bruinsma, Theory of hydrodynamic convection in soap films. *Physica A* 216 (1995) 59–76.
17. C.J.W. Breward, *The Mathematics of Foam*. Oxford University: D. Phil. Thesis (1999) 184 pp.
18. S. A. Snow and R. E. Stevens, 'The science of silicone surfactant application in the formation of polyurethane foam.' In: R.H. Hill (ed.), *Silicone Surfactants*, (Surfactant Science Series, vol. 86), New York: Marcel Dekker, Inc. (1999) pp. 137–158.
19. D. Myers, *Surfactant Science and Technology*. New York: VCH Publishers (1988) 351 pp.
20. K.J. Stebe and C. Maldarelli, Remobilizing surfactant retarded fluid particle interfaces. II: controlling the surface mobility at interfaces of solutions containing surface active components. *J. Colloid Interf. Sci.* 163 (1994) 177–189.
21. S. A. Snow, U. C. Pernisz and R. E. Stevens, Thin liquid model polyurethane films. In: Proc. Technical/Marketing Conf., Polyurethane Expo /98, Dallas, Texas 1998, Am. Plastics Council, Arlington, VA, USA (1998) pp. 1–10.
22. Dow Corning, unpublished research.
23. J.B.M. Hudales and H.N. Stein, Profile of the plateau border in a vertical free liquid film. *J. Colloid Interf. Sci.* 137 (1989) 512–526.
24. H.N. Stein, On marginal regeneration. *Adv. Colloid Interf. Sci.* 34 (1991) 175–190.
25. J.B.M. Hudales and H.N. Stein, Marginal regeneration of a mobile vertical free liquid film. *J. Colloid Interf. Sci.* 138 (1990) 354–364.
26. V.A. Nierstrasz and G. Frens, Marginal regeneration in thin vertical liquid films. *J. Colloid Interf. Sci.* 207 (1998) 209–217.
27. V.A. Nierstrasz and G. Frens, Marginal regeneration and the Marangoni effect. *J. Colloid Interf. Sci.* 215 (1999) 28–35.
28. R. J. Braun, S. A. Snow and U. C. Pernisz, Gravitational drainage of a tangentially-immobile thick film. *J. Colloid Interf. Sci.* 219 (1999) 225–240.
29. S. Naire, R. J. Braun and S. A. Snow, An insoluble surfactant model for a vertical draining free film. *J. Colloid Interf. Sci.* 230 (2000) 91–106.
30. S. Naire, R.J. Braun and S.A. Snow, An insoluble surfactant model for a vertical draining free film with variable surface viscosity. *Phys. Fluids* 13 (2001) 2492–2502.
31. S. Naire, *Gravitationally-Driven Drainage of Thin Films.* University of Delaware: Ph.D. Thesis (2000) 224 pp.
32. L.W. Schwartz and R.V. Roy, Modeling draining flow in mobile and immobile soap films. *J. Colloid Interf. Sci.* 218 (1999) 309–324.

33. R. J. Braun, S. A. Snow and U. C. Pernisz, Developing a physical model of a draining vertically alligned thin liquid (soap) film: Part II: free surface model. Dow Corning Corporation Research Report 1998-I0000-45018 (1998).
34. L.W. Schwartz and D.E. Weidner, An analysis of the effect of surfactant on the leveling behavior of a thin liquid coating layer. *Langmuir* 11 (1995) 3690–3693.
35. L.W. Schwartz, R.A. Cairncross and D.E. Weidner, Anomalous behavior during leveling of thin coating layers with surfactant. *Phys. Fluids* 8 (1996), 1693–1695.
36. C.-W. Park, Effects of insoluble surfactants on dip coating. *J. Colloid Interf. Sci.* 146 (1991) 382–394.
37. Y.P. Pawar and K.J. Stebe, Marangoni effects on drop deformation in an extensional flow: The role of surfactant physcial chemistry. I. Insoluble surfactants. *Phys. Fluids* 8 (1996) 1738–1751.
38. C.D. Eggleton, Y.P. Pawar and K.J. Stebe, Insoluble surfactants on a drop in an extentsional flow: A generalization of the stagnated surface limit to deforming interfaces. *J. Fluid Mech.* 385 (1999) 79–99.
39. S. Naire, R. J. Braun and S. A. Snow, Limiting cases of gravitational drainage of a vertical free film for evaluating surfactants. *SIAM J. Appl. Math.* 61 (2000) 889–913.
40. L.E. Scriven, Dynamics of a fluid interface: Equation of motion for Newtonian surface fluids. *Chem. Eng. Sci.* 12 (1960) 98–108.
41. D. A. Edwards, H. Brenner and D. T. Wasan, *Interfacial Transport Processes and Rheology*. Boston: Butterworth-Heinemann (1991) 558 pp.
42. J.C. Slattery, *Interfacial Transport Phenomena*. New York: Springer-Verlag (1990) 1159 pp.
43. H.A. Stone, A simple derivation of the time-dependent convective-diffusion equation for surfactant transport along a deforming interface. *Phys. Fluids A* 2 (1990) 111–113.
44. H. Wong, D. Rumschitzki and C. Maldarelli, On the surfactant mass balance at a deforming fluid interface. *Phys. Fluids* 8 (1996) 3203–3204.
45. J.M. Lopez and A. Hirsa, Surfactant-influenced gas-liquid interfaces: nonlinear equation of state and finite surface viscosities. *J. Colloid Interf. Sci.* 229 (2000) 575–583.
46. J.M. Lopez and A. Hirsa, Direct determination of the dependence of the surface shear and dilatational viscosities on the thermodynamic state of the interface: theoretical foundations. *J. Colloid Interf. Sci.* 206 (1998) 231–239.
47. C.F. Brooks, G.G. Fuller, C.W. Frank and C.R. Robertson, An interfacial stress rheometer to study rheological transitions in monolayers at the air-water interface. *Langmuir* 15 (1999) 2450–2459.
48. C.A. Naumann, C.F. Brooks, G.G. Fuller, W. Knoll and C.W. Frank, Viscoelastic properties of lipopolymers at the air-water interface: a combined interfacial stress rheometer and film balance study. *Langmuir* 15 7752 (1999) 7752–7761.
49. G.L. Gaines, *Insoluble Monolayers at Liquid-Gas Interfaces*. New-York: Interscience (1966) 386 pp.
50. S.D.R. Wilson, The drag-out problem in film coating theory. *J. Eng. Math.* 16 (1982) 209–221.
51. H.S. Kheshgi, S.F. Kistler and L.E. Scriven, Rising and falling film flows: viewed from a first order approximation. *Chem. Eng. Sci.* 47 (1992) 683–694.
52. K.J. Ruschak, Flow of a falling film into a pool. *AIChE J.* 24 (1978) 705–708.
53. T. Erneux and S.H. Davis, Nonlinear rupture of free films, *Phys. Fluids A* 5 (1993) 1117–1122.
54. M.P. Ida and M.J. Miksis, Thin film rupture. *Appl. Math. Lett.* 9 (1996) 35–40.
55. M.P. Ida and M.J. Miksis, The dynamics of thin films I: general theory. *SIAM J. Appl. Math.* 58 (1998) 456–473.
56. M.P. Ida and M.J. Miksis, The dynamics of thin films II: applications. *SIAM J. Appl. Math.* 58 (1998) 474–500.
57. A. De Wit, D. Gallez and C.I. Christov, Nonlinear evolution equations for thin liquid films with insoluble surfactants. *Phys. Fluids* 6 (1994) 3256–3266.
58. O.E. Jensen, Self-similar, surfactant-driven flows. *Phys. Fluids* 6 (1994) 1084–1094.
59. K.E. Brennan, S.L. Campbell and L.E. Petzold, *Numerical Solution of Initial-Value Problems in Differential-Algebraic Systems*. Philadelphia: SIAM (1996) 256 pp.
60. O.E. Jensen, The thin liquid lining of a weakly curved cylindrical tube. *J. Fluid Mech.* 331 (1997) 373–403.
61. S.A. Snow, U.C. Pernisz and B.M. Nugent, The drainage of thin, vertical, model polyurethane liquid films, dow corning corporation research report (1999) in preparation.
62. G.B. Whitham, *Linear and Nonlinear Waves.* New York: Wiley-Interscience (1974) 636 pp.
63. J.B. Grotberg and D.P. Gaver, A synopsis of surfactant spreading research. *J. Colloid Interf. Sci.* 178 (1996) 377–379.

64. S. A. Snow, U. C. Pernisz and B. M. Nugent, Cell opening in polyurethane films part III: the drainage of thin liquid model polyurethane films. Dow Corning Corporation Research Report 1996-I0000-41395 (1996).
65. E.B. Hansen, Stokes flow down a wall into an infinite pool. *J. Fluid Mech.* 178 (1987) 243−256.
66. S.F. Kistler and P.M. Schweizer (eds.), *Liquid Film Coating: Scientific Principles and Their Technological Implications*. London: Chapman and Hall (1997) 783 pp.
67. S. Naire, R.J. Braun and S.A. Snow, A 2+1 dimensional model for vertical free film drainage. Submitted.